Neurobiology of Disease 130 (2019) 104525

Contents lists available at ScienceDirect

Neurobiology of Disease

journal homepage: www.elsevier.com/locate/ynbdi

Time course and magnitude of alpha-synuclein inclusion formation and nigrostriatal degeneration in the rat model of synucleinopathy triggered by intrastriatal α-synuclein preformed fibrils

Joseph R. Patterson[a,*], Megan F. Duffy[a,b], Christopher J. Kemp[a], Jacob W. Howe[a], Timothy J. Collier[a,b,c], Anna C. Stoll[a,d], Kathryn M. Miller[a,b], Pooja Patel[a], Nathan Levine[e], Darren J. Moore[e], Kelvin C. Luk[f], Sheila M. Fleming[g], Nicholas M. Kanaan[a,b,c], Katrina L. Paumier[a], Omar M.A. El-Agnaf[h], Caryl E. Sortwell[a,b,c]

[a] Department of Translational Neuroscience, Michigan State University, Grand Rapids, MI, USA
[b] Neuroscience Program, Michigan State University, East Lansing, MI, USA
[c] Mercy Health Hauenstein Neuroscience Medical Center, Grand Rapids, MI, USA
[d] Department of Pharmacology and Toxicology, Michigan State University, East Lansing, MI, USA
[e] Center of Neurodegenerative Science, Van Andel Institute, Grand Rapids, MI, USA
[f] Center for Neurodegenerative Disease Research, Department of Pathology and Laboratory Medicine, University of Pennsylvania Perelman School of Medicine, Philadelphia, PA, USA
[g] College of Pharmacy, Northeast Ohio Medical University, Rootstown, OH, USA
[h] Neurological Disorders Researcher Center, Qatar Biomedical Research Institute (QBRI), Hamad Bin Khalifa University (HBKU), Qatar Foundation, Doha, Qatar

ARTICLE INFO

Keywords:
Alpha-Synuclein
Preformed fibrils
Synucleinopathy
Parkinson's disease

ABSTRACT

Animal models that accurately recapitulate the accumulation of alpha-synuclein (α-syn) inclusions, progressive neurodegeneration of the nigrostriatal system and motor deficits can be useful tools for Parkinson's disease (PD) research. The preformed fibril (PFF) synucleinopathy model in rodents generally displays these PD-relevant features, however, the magnitude and predictability of these events is far from established. We therefore sought to optimize the magnitude of α-syn accumulation and nigrostriatal degeneration, and to understand the time course of both. Rats were injected unilaterally with different quantities of α-syn PFFs (8 or 16 μg of total protein) into striatal sites selected to concentrate α-syn inclusion formation in the substantia nigra pars compacta (SNpc). Rats displayed an α-syn PFF quantity-dependent increase in the magnitude of ipsilateral SNpc inclusion formation at 2 months and bilateral loss of nigral dopamine neurons at 6 months. Unilateral 16 μg PFF injection also resulted in modest sensorimotor deficits in forelimb adjusting steps associated with degeneration at 6 months. Bilateral injection of 16 μg α-syn PFFs resulted in symmetric bilateral degeneration equivalent to the ipsilateral nigral degeneration observed following unilateral 16 μg PFF injection (~50% loss). Bilateral PFF injections additionally resulted in alterations in several gait analysis parameters. These α-syn PFF parameters can be applied to generate a reproducible synucleinopathy model in rats with which to study pathogenic mechanisms and vet potential disease-modifying therapies.

1. Introduction

Parkinson's disease (PD) is the second most common neurodegenerative disease, estimated to affect one out of every hundred individuals over the age of sixty, and expected to rise to 1,238,000 cases in the United States by 2030 (Dorsey et al., 2007; Marras et al., 2018). Motor impairment in PD are associated with progressive degeneration of nigrostriatal dopamine neurons, and the accumulation of intracellular Lewy Bodies (LBs), of which the protein alpha-synuclein (α-syn) is the principal component (Graybiel et al., 1990; Pollanen et al., 1993; Spillantini et al., 1997; Fahn, 2003; Jankovic, 2008).

Neurotoxicant models of parkinsonism, such as 1 methyl-4-phenyl 1, 2, 3, 6-tetrahydropyridine (MPTP) and 6-hydroxydopamine (6-OHDA), demonstrate marked nigrostriatal loss and motor impairment. However, these models tend to lack the protracted and sequential progression associated with PD and show limited signs of α-syn

* Corresponding author.
E-mail address: Joseph.Patterson@hc.msu.edu (J.R. Patterson).

https://doi.org/10.1016/j.nbd.2019.104525
Received 9 January 2019; Received in revised form 21 June 2019; Accepted 1 July 2019
Available online 02 July 2019

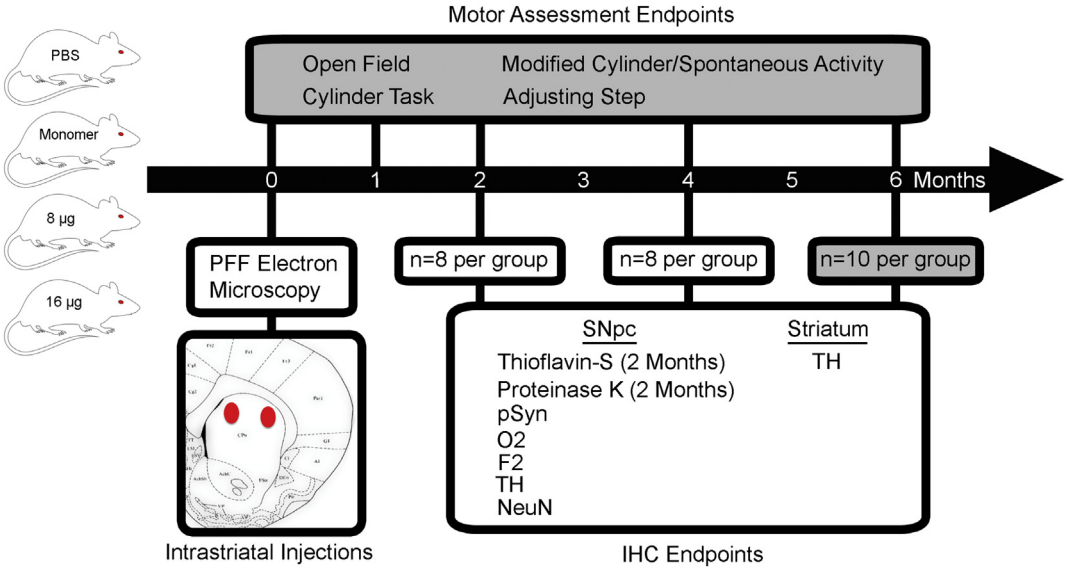

Fig. 1. Experimental Design and Endpoints. Rats were injected with either phosphate buffered saline (PBS) vehicle, 16 µg α-syn monomers (6-month cohort only), or 8 or 16 µg α-syn PFFs. Prior to intrastriatal injections (locations of injections denoted in red), monomers and fibrils were examined with transmission electron microscopy to verify appropriate fibril size after sonication. Brains were collected at 2, 4, and 6-months p.i. for IHC endpoints. IHC endpoints measured in the SNpc were thioflavin-S staining and proteinase K resistance (2-month time point only), pSyn, O2, F2, TH, and NeuN. IHC endpoint measured in the striatum was TH. In the 6-month cohort (shaded in gray) prior to injection and 1, 2, 4, and 6-months after injection motor assessments were performed via open field, cylinder test, modified cylinder/spontaneous activity, and adjusting step.

Abbreviations: µg; microgram; α-syn = alpha-synuclein; PBS = phosphate buffered saline; PFFs = α-syn preformed fibrils; p.i. = post-injection; IHC = immunohistochemistry; SNpc = substantia nigra pars compacta; pSyn = α-syn phosphorylated at serine 129; O2 = α-syn oligomers and fibrils; F2: α-syn fibrils only; TH = tyrosine hydroxylase; NeuN = neuronal nuclei. (For interpretation of the references to colour in this figure legend, the reader is referred to the web version of this article.)

pathology (Dauer and Przedborski, 2003; Forno et al., 1993). Transgenic α-syn models demonstrate robust accumulation of α-syn inclusions over long intervals but almost always lack nigrostriatal degeneration (Matsuoka et al., 2001; Gomez-Isla et al., 2003; Nuber et al., 2013). Overexpression of wildtype and mutant human α-syn mediated by viral vector delivery results in an abbreviated interval of α-syn accumulation followed by rapid, titer-dependent nigrostriatal degeneration and motor deficits (Gombash et al., 2013). However in both α-syn transgenics and viral vector models, neurotoxicity is driven by supraphysiological levels of α-syn, levels not normally present in idiopathic PD (Neystat et al., 1999; Kirik et al., 2002; Klein et al., 2002; Lo Bianco et al., 2002; Kingsbury et al., 2004; Yamada et al., 2004; Tan et al., 2005; Grundemann et al., 2008; Ulusoy et al., 2010; Zhou et al., 2011; Lundblad et al., 2012; Mulcahy et al., 2012; Oliveras-Salva et al., 2013; Van der Perren et al., 2015; Volpicelli-Daley et al., 2016; Ip et al., 2017; Su et al., 2017; Duffy et al., 2018a). Of central importance, the majority of therapeutics developed and tested in these models have failed to effectively translate to humans (Potashkin et al., 2010; Munoz et al., 2016; Zeiss et al., 2017).

In vitro and In vivo exposure to sonicated α-syn preformed fibrils (PFFs) results in the PFFs being taken up into neurons where they initiate templating, phosphorylation, accumulation, and subsequent formation of α-syn inclusions within the context of normal levels of endogenous α-syn (Volpicelli-Daley et al., 2011; Luk et al., 2012; Volpicelli-Daley et al., 2014; Osterberg et al., 2015; Paumier et al., 2015; Duffy et al., 2018b). Injected PFFs are not intrinsically toxic, requiring templating of endogenous α-syn for inclusions to form and for degeneration to occur (Volpicelli-Daley et al., 2011; Luk et al., 2012; Volpicelli-Daley et al., 2014). When injected into the striatum of rats or mice, α-syn PFFs trigger the formation of inclusions in the ipsilateral substantia nigra pars compacta (SNpc) within weeks post-injection (p.i.). These inclusions are immunoreactive for α-syn phosphorylated at serine 129 (pSyn) (Volpicelli-Daley et al., 2011; Luk et al., 2012; Paumier et al., 2015; Duffy et al., 2018b). Additionally, inclusions share similar properties with LBs, they contain pSyn, ubiquitin, are proteinase K-resistant, and are thioflavin positive (Paumier et al., 2015; Osterberg et al., 2015; Duffy et al., 2018b). Inclusions also accumulate in other brain regions that directly innervate the striatum, most prominently in the cingulate, insular and motor cortices, amygdala, and thalamus (Luk et al., 2012; Wall et al., 2013; Paumier et al., 2015; Duffy et al., 2018). Decreases in striatal tyrosine hydroxylase (TH) and dopamine, and neurodegeneration of the nigrostriatal pathway are observed subsequent to inclusion formation with significance by six months post-injection (Luk et al., 2012; Paumier et al., 2015; Duffy et al., 2018b). Interestingly, degeneration is not ipsilaterally-limited in rats, as contralateral nigrostriatal neurons degenerate independent of apparent inclusion formation (Paumier et al., 2015; Duffy et al., 2018b).

Overall, the protracted synucleinopathy and neurodegeneration induced following intrastriatal α-syn PFF injection is an attractive model for preclinical PD research. However, thus far the model is limited in several ways. First, the magnitude of nigrostriatal degeneration from intrastriatal injections to date ranges from 35 to 41% (Luk et al., 2012; Luk et al., 2016; Paumier et al., 2015; Duffy et al., 2018b). Optimization of α-syn PFF injection parameters and careful systematic characterization of the magnitude and time course of pathological events in this model can be leveraged to study specific pathological phenomena at specific post-injection intervals. The α-syn PFF model also could be further improved by amplified nigrostriatal neurodegeneration since the maximal nigral dopamine neuron loss reported following intrastriatal α-syn PFF injection into rats or mice to date has been ~35% (Luk et al., 2012; Paumier et al., 2015; Duffy et al., 2018b). This is an inadequate level of degeneration to induce robust motor phenotypes. Reports of behavioral deficits in PFF-injected rats or mice are limited to impairment in ultrasonic vocalization or in muscle coordination or endurance as indicated by rotarod and wire hang test, respectively (Luk et al., 2012; Paumier et al., 2015).

In the present series of experiments, we sought to optimize the intrastriatal α-syn PFF model using two specific modifications to our

previously published parameters (Paumier et al., 2015; Duffy et al., 2018b). First, striatal injection coordinates were altered to increase the proportion of nigrostriatal terminal fields targeted (Lerner et al., 2015) in order to improve SNpc inclusion yield, sparing the neighboring ventral tegmental area (Polinski et al., 2018). Second, we increased the amount of total PFF protein injected, as the optimal concentration of template provided by the PFFs is yet unknown. In this study, rats were injected unilaterally into two sites in the striatum with a total of 8 or 16 μg of mouse α-syn PFFs and assessed over a 6 month time course for the magnitude of SNpc inclusion formation, nigrostriatal degeneration, and motor deficits (Fig. 1). Inclusions within the SNpc were further examined to expand on our understanding of the conformations of α-syn inclusions over time. Previously in the model, inclusions were primarily detected based on the presence of pSyn. Conformation specific antibodies were used to detect oligomeric and fibrillar forms of α-syn over time to better understand the dynamics of α-syn within the model.

In human PD, loss of the axon terminals of the nigrostriatal dopamine neurons can precede soma loss (Kordower et al., 2013). Likewise, evidence from individuals with incidental Lewy body disease, which may be representative of early PD, suggests pathways involved in axonal dysfunction are altered (Dijkstra et al., 2015). As such, the study also explored whether early deficits in striatal terminals occur. As intrastriatal PFF injections produce early compensatory increases in TH in the striatum, followed by a subsequent sustained decrease, markers of dopamine terminals throughout the progression of the synucleinopathy are of interest (Paumier et al., 2015). To address this, the temporal TH expression in the striatum was examined in relation to degeneration in the SNpc.

In a follow-up study rats were bilaterally injected into the striatum with 16 μg of mouse α-syn PFFs and examined over the same 6-month time course (Fig. 2). Since unilateral intrastriatal PFF injections produce eventual contralateral degeneration (Paumier et al., 2015; Duffy et al., 2018), we sought to explore whether bilateral administration of PFFs could enhance this cross-hemisphere effect and increase nigral degeneration. The use of bilateral PFF injections may also produce non-motor effects that could be further examined in the future.

Our results show an α-syn PFF quantity-dependent increase in the magnitude of inclusion formation at 2 months in SNpc ipsilateral to each injection, and bilateral loss of nigral dopamine neurons at 6 months. Bilateral injection of 16 μg α-syn PFFs resulted in symmetric bilateral degeneration equivalent to the ipsilateral nigral degeneration observed following unilateral 16 μg PFF injection (~50% loss). Bilateral PFF injections also resulted in alterations in several gait analysis parameters. Application of these modified parameters can be used to generate a reproducible nigrostriatal synucleinopathy model in rats with which to study pathogenic mechanisms and vet potential disease-modifying therapies.

2. Materials and methods

2.1. Experiment 1 overview

Experiment 1 was designed to examine the effects of increasing the quantity of α-syn PFFs unilaterally injected at optimized intrastriatal coordinates. Rats received either PBS (vehicle), 16 μg mouse α-syn monomers (6 month cohort only), 8 or 16 μg mouse α-syn PFFs. Immunohistochemical (IHC) endpoints were measured at 2, 4, and 6 months post-injection (p.i.). Quantification of pSyn, α-syn oligomers and fibrils (O2), α-syn fibrils (F2), TH, and neuronal nuclei (NeuN) was performed in the SNpc. Additionally, thioflavin-S staining and proteinase K resistance was assessed within the two month cohort. TH was measured in the striatum by near infrared imaging. Motor assessments were evaluated at 1, 2, 4, and 6 months p.i. within the 6-month cohort using distance traveled in an open field, cylinder test, modified cylinder/spontaneous activity, and adjusting step test (Fig. 1).

2.2. Experiment 2 overview

Experiment 2 was designed to examine the impact of bilateral

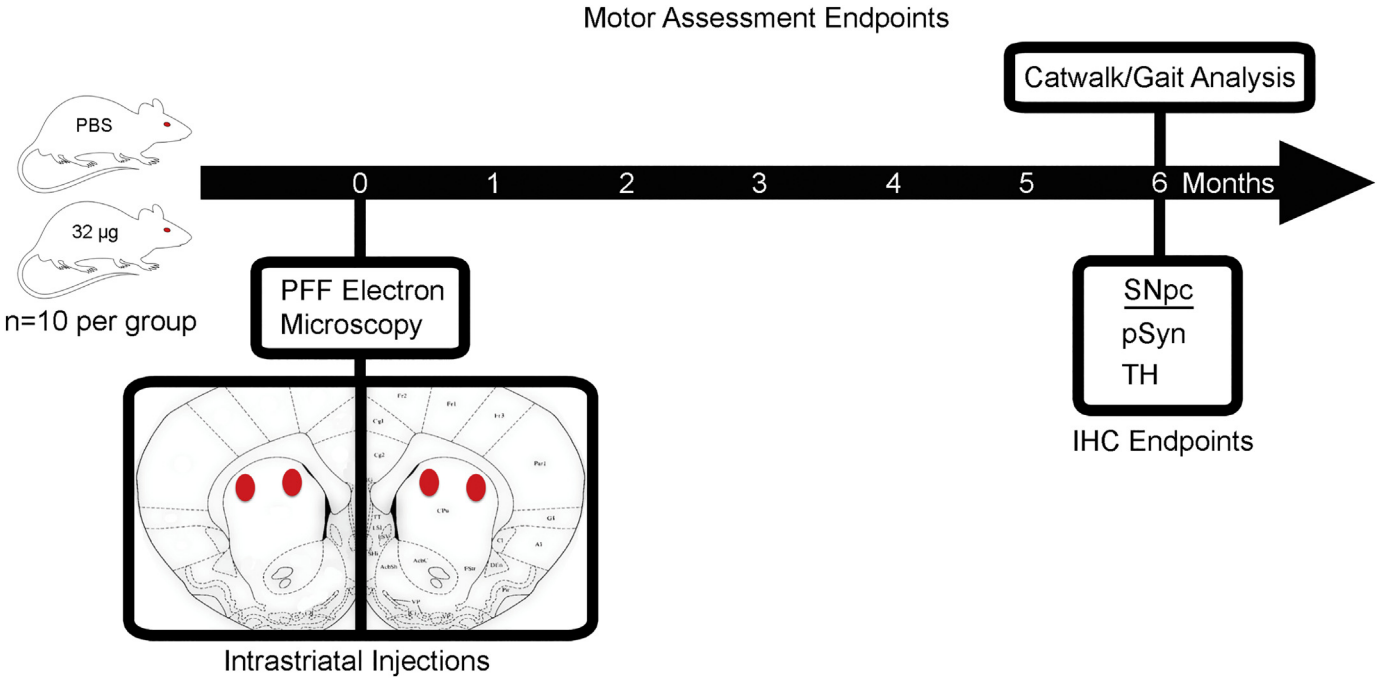

Fig. 2. Experimental Design and Endpoints. Rats were injected with either phosphate buffered saline (PBS) vehicle or 16 μg alpha-synuclein preformed fibrils (α-syn PFFs) per side. Prior to intrastriatal injections (locations of injections denoted in red), fibrils were examined with transmission electron microscopy for quality assurance. Brains were collected 6-months post-injection (p.i.) for immunohistochemical (IHC) endpoints. IHC endpoints measured in the substantia nigra pars compacta (SNpc) were phosphorylated α-syn at serine 129 (pSyn) and tyrosine hydroxylase (TH). Motor assessments were performed via catwalk/gait analysis at 6 months. (For interpretation of the references to colour in this figure legend, the reader is referred to the web version of this article.)

intrastriatal PFF injections on nigrostriatal neurodegeneration and motor impairment. Rats received either PBS (vehicle) or 16 μg mouse α-syn PFFs per side. Quantification of pSyn and TH was performed in the SNpc at 6 months p.i. Likewise, motor assessments were performed at 6 months p.i. using catwalk/gait analysis (Fig. 2).

2.3. Animals

Three-month-old, male Fischer 344 rats ($n = 88$ unilateral injections; $n = 20$ bilateral injections) were obtained from Charles River Laboratories. Rats were housed 1–2 to a cage in a room with a 12 h light/dark cycle and provided food and water ad libitum. All work was performed at the AAALAC accredited Van Andel Research Institute vivarium with specific approval from the Michigan State Institutional Animal Care and Use Committee.

2.4. α-syn PFF preparation and quality control

Fibrils were generated using wild-type, full-length, recombinant mouse α-syn monomers as previously described (Volpicelli-Daley et al., 2011; Luk et al., 2012; Volpicelli-Daley et al., 2014; Polinski et al., 2018). Quality control was performed on full length fibrils to confirm fibril formation (transmission electron microscopy), amyloid structures within fibrils (thioflavin T assay), a shift to higher molecular weight species compared to monomers (sedimentation assay), and low bacterial contamination (< 0.5 endotoxin units mg^{-1} of total protein via a *Limulus* amebocyte lysate assay). On the day of surgery, PFFs were thawed to room temperature (RT) diluted to either 2 or 4 μg ul^{-1} in Dulbecco's phosphate buffered saline (DPBS) (Gibco, 14,190–136), and sonicated at RT using an ultrasonic homogenizer (300 VT; Biologics, Inc.) for 60, 1 s pulses with the pulser set at 20% and power output set at 30%. Prior to surgeries, an aliquot of sonicated PFFs was analyzed using transmission electron microscopy.

2.5. Electron microscopy

Samples were prepared on Formvar/carbon-coated copper grids (EMSDIASUM, FCF300-Cu). Grids were washed twice by floating grids on drops of ddH_2O. Grids were floated for 1 min on 10 μl drops of sonicated PFFs diluted 1:50 in PBS, followed by 1 min on 10 μl drops of aqueous 2% uranyl acetate, wicking away liquid with filter paper after each step. Grids were allowed to dry before imaging with a JEOL JEM-1400+ transmission electron microscope. Pre-surgery, a brief assessment of fibril size was performed by measuring 20 representative fibrils to ensure fibril length was approximately 50 nm, a length known to produce optimal seeding (Tarutani et al., 2016; Abdelmotilib et al., 2017). Post-surgery, the length of over 500 fibrils per sample was measured, and the average length and the size distribution plotted. Post-surgery measurements were performed with the measure tool in Adobe Photoshop (CS2) and final fibrils sizes calculated based on the scalebar associated with the image.

2.6. Stereotaxic surgeries

In *Experiment 1* rats were anesthetized with isoflurane and 2 μl injections were performed unilaterally into two striatal sites (AP +1.6, ML +2.0, DV -4.0; AP +0.1, ML +4.2, DV -5.0). Coordinates were selected based on modifications of coordinates demonstrated in mice to target the axon terminals of SNpc neurons specifically (Lerner et al., 2015; Polinski et al., 2018). In *Experiment 2*, rats were injected bilaterally, using the coordinates in *Experiment 1*, however, injections were made into both hemispheres (total of four 2 μl injections, AP +1.6, ML ± 2.0, DV -4.0; AP +0.1, ML ± 4.2, DV -5.0). Injections were performed using pulled glass needles attached to 10 μl Hamilton syringes at a flow rate of 0.5 μl min^{-1}. At the end of each injection, needles were left in place for 1 min, withdrawn 0.5 mm, left in place an additional 2 min to avoid displacement of PFFs, and retracted. Unilateral injections consisted of PBS (vehicle control), 4 μg μl^{-1} monomeric α-syn (16 μg of total protein), 2 μg μl^{-1} (8 μg of total protein) or 4 μg μl^{-1} (16 μg of total protein) of α-syn PFFs. Bilateral injections consisted of PBS or 4 μg μl^{-1} (16 μg per side, 32 μg total protein). During surgeries, PBS and PFFs were kept at RT and monomeric α-syn kept on ice until use. Post-surgery, animals received an analgesic (1.2 mg kg^{-1} of sustained release buprenorphine) and were monitored until euthanized. Unilaterally injected rats in *Experiment 1* were euthanized at 2 months (60 days), 4 months (120 days), or 6 months (180 days) p.i. based on the time course of synucleinopathy and degeneration observed previously (Paumier et al., 2015; Duffy et al., 2018b). At the 2- and 4-month time points there were 8 rats per group, and group size was increased to 10 rats/group for sensorimotor testing at the 2, 4 and 6-month time points and euthanized at 6 months (Fig. 1). Bilaterally injected rats in *Experiment 2* were tested for sensorimotor function and euthanized at 6 months (180 days) p.i., with 10 rats per group included in this study (Fig. 2).

2.7. Immunohistochemistry

Rats were euthanized with a pentobarbital (Beuthanasia-D Special, Merck Animal Health) overdose (30 mg kg^{-1}) and intracardially perfused with cold heparinized saline (0.9%), followed by 4% paraformaldehyde in 0.1 M phosphate buffer (pH 7.3). Brains were post-fixed in 4% paraformaldehyde for at least 48 h, and cryoprotected in 30% sucrose. Brains were mounted on a chilled platform, frozen using dry ice and sectioned on a sliding microtome. A 1:6 series of sections (40 μm thick), were collected in cryoprotectant (30% sucrose, 30% ethylene glycol, in tris buffered saline (TBS) pH 7.3) and stored at −20 °C. Sections were washed 4 × 5 min in TBS containing 0.5% Triton-X100 (TBS-Tx), cleared 1 h in 0.3% H_2O_2, blocked for 1 h in 10% normal goat serum (NGS) in TBS-Tx, and incubated overnight at 4 °C in primary antibody in 1% NGS/TBS-Tx. Primary antibodies used were 1:10000 mouse anti-phosphorylated α-syn at serine 129 (Abcam, AB184674), 1:4000 rabbit anti-tyrosine hydroxylase (Millipore, AB152), 1:5000 mouse anti-neuronal nuclei (Millipore, MAB377), 1:5000 mouse anti-α-syn oligomers/fibrils (O2) (Vaikath et al., 2015), and 1:5000 mouse anti-α-syn fibrils (F2) (Vaikath et al., 2015). Sections were washed in TBS-Tx and incubated for 2.5 h in either goat anti-mouse (Millipore, AP124B) or goat anti-rabbit (Millipore, AP132B) biotinylated secondary antibodies (diluted 1:500 in 1% NGS/TBS-Tx). Sections were washed in TBS-Tx, and incubated for 2 h using standard avidin-biotin complex detection kit (ABC; Vector Laboratories, PK-6100). Sections were developed using 2.5 mg ml^{-1} nickel ammonium sulfate hexahydrate (Fisher, N48–500), 0.5 mg ml^{-1} diaminobenzidine (Sigma-Aldrich, D5637), and 0.03% H_2O_2 in TBS-Tx. After washing in TBS-Tx, sections were mounted, allowed to dry, rehydrated in ddH_2O, dehydrated in a graded ethanol series, followed by xylene, and coverslipped using Cytoseal (Thermo-Fisher, 22–050-262). The sections containing the SNpc were counterstained with cresyl violet to visualize intraneuronal pSyn inclusions. All samples within a post-surgical time point were processed simultaneously with the same batch of antibody to minimize variability. Representative images were taken with a Nikon Eclipse 90i microscope with a Nikon DS-Ri1 colour camera using Nikon Elements AR (Version 4.50.00, Melville, NY) software.

2.8. Immunofluorescence

Nigral sections were washed in TBS-Tx 4 × 5 min, blocked 1 h in 10% NGS in TBS-Tx, and incubated overnight at 4 °C in primary antibody in 1% NGS/TBS-Tx. Primary antibodies used were 1:5000 mouse (IgG1 isotype) anti-NeuN (Millipore, MAB377), 1:10000 mouse (IgG2α isotype) anti-phosphorylated α-syn at serine 129 (Abcam, AB184674), and 1:4000 rabbit anti-TH (Millipore, AB152). Sections were washed with TBS-Tx and incubated 2 h at RT. Secondary antibodies Alexa Fluor

488 goat anti-mouse IgG1 (Invitrogen, A21121), Alexa Fluor 594 goat anti-mouse IgG2α (Invitrogen, A21135), or Alexa Fluor 488 goat-anti rabbit (Invitrogen, A11034) were used. Sections were washed in TBS, mounted, and coverslipped with Vectashield hard set mounting medium (Vector Laboratories, H-1400). Images were taken with a Nikon Eclipse 90i microscope with a QICAM camera (QImaging, Surrey, British Columbia, Canada), using Nikon Elements AR (Version 4.50.00, Melville, NY) software.

2.9. Proteinase-K digestion

A 1:12 series of sections containing the SNpc was washed 6 × 5 min in TBS (pH 7.6). A subset of sections was treated with 10 μg ml^{-1} proteinase K (Invitrogen, 25,530,015) for 30 min at RT. Following proteinase K digestion, sections were washed in TBS-Tx, and were processed for immunohistochemistry as described above. A pan rabbit anti-α-syn primary was used at 1:1000 (Abcam, AB15530). Sections were mounted, dehydrated, and coverslipped as described above. Representative images were taken with a Nikon Eclipse 90i microscope with a Nikon DS-Ri1 colour camera using Nikon Elements AR (Version 4.50.00, Melville, NY) software.

2.10. Thioflavin S staining

A 1:12 series of sections containing the SNpc was washed 4 × 5 min in TBS (pH 7.3), mounted on subbed slides, and allowed to dry for at least an hour. Samples were incubated for 25 min in 0.5% potassium permanganate (Sigma-Aldrich, 223,468) in TBS to quench auto-fluorescence. Sections were washed in TBS, destained 3 min in 0.2% potassium disulfite (Sigma-Aldrich, P2522) and 0.2% oxalic acid (Sigma-Aldrich, 75,688) in TBS, and stained for 3 min in 0.0125% thioflavin-S in 40% ethanol/60% TBS (Sigma-Aldrich, T1892). Sections were differentiated in 50% ethanol/50% TBS, washed 5 × 5 min in TBS, washed 3 × 5 min in ddH_2O, and coverslipped with Vectashield hard set mounting media (Vector Laboratories, H-1400). Images were taken with a Nikon Eclipse 90i microscope with a QICAM camera (QImaging, Surrey, British Columbia, Canada), using Nikon Elements AR (Version 4.50.00, Melville, NY) software.

2.11. TH near infrared immunofluorescence of Nigral terminals in the striatum

Striatal sections were washed in TBS 4 × 5 min and blocked 1 h in StartingBlock T20 (Thermo-Fisher, 37,543). Sections were incubated overnight in 1:1000 mouse anti-TH (Millipore, MAB318). Following washes with TBS, sections were incubated in 1:500 donkey anti-mouse 680LT IRDye (LiCor #926–68,022) for 2 h in the dark. To avoid batch or dilution variations, all samples from each timepoint were processed simultaneously, and all solutions were diluted in a single container and aliquoted prior to use. Sections were washed in TBS, mounted, and coverslipped with Vectashield hard set mounting media (Vector Laboratories, H-1400). Slides were imaged on a LiCor Odyssey CLx flatbed scanner. Images were analyzed in Image Studio Lite Version 5.2. Contours were drawn around both hemispheres of the striatum of six sections, and the fluorescence intensity measured in the 700 channel. The striatal contours were defined by the corpus callosum and lateral ventricles, with the ventral contour cutoff at the bottom of the lateral ventricle. From each slide, a box was drawn on the cortex, the signal within the box was used to subtract background fluorescence. Group means and standard error of the mean (SEM) were calculated using each section as a data point, rather than averaging the means of individual rats within each group.

2.12. Quantification of α-syn inclusion-bearing neurons in the SNpc

Total enumeration of neurons containing pSyn, O2, and F2, was performed using Microbrightfield Stereoinvestigator (MBF Bioscience). Sections containing the SNpc (1:6 series) were used for all counts with an investigator blinded to treatment groups. Contours were drawn around the SNpc using the 4× objective. A 20× objective was used to identify stained cells and a marker placed. Stained cells for total enumeration were defined as dark staining either throughout the cell soma or as distinct puncta. The sections used to quantify pSyn were counterstained with cresyl violet to identify neurons and pSyn was quantified within cells, as to not over-estimate inclusion-containing cells in the cases where multiple puncta in close proximity are present. Non-specific staining within blood vessels was excluded from the final counts. Total counts for each animal were multiplied by six to estimate the total number of neurons in each animal with inclusions.

2.13. Stereology

Unbiased stereology was performed with Microbrightfield Stereoinvestigator (MBF Bioscience) using the optical fractionator probe. Sections containing the SNpc (1:6 series) were used for all counts. In all cases, the investigator was blinded to treatment groups. Contours were drawn around the SNpc using the 4× objective. Stereology was performed with TH and NeuN to estimate the total population in the SNpc. A grid (183 μm × 112 μm) was placed over the drawn contour, and counting boxes (50 μm × 50 μm) were randomly selected by the program to quantify approximately 20% of the SNpc. Guard zone was set at 3 μm, optical dissector height at 23 μm, and sections measured every third counting box, with the normal measured section thickness being approximately 30 μm. TH or NeuN labeled neurons within the counting frame were counted while focusing through a z-stack. Counts were performed using a 60× oil immersion objective and estimates of total stained neurons were calculated with the optical fractionator. Variability was assessed with the Gundersen coefficient of error (≤0.1). Any sample where the SNpc was obscured in two or more sections, such as by a tear in the section, was excluded.

2.14. Sensorimotor testing

In *Experiment 1* unilaterally injected rats were assessed for forelimb use asymmetry in the cylinder test, spontaneous activity in the cylinder, locomotor activity in the open field and forelimb use in the adjusting step test. Assessments were made prior to surgery (baseline), and at 1, 2, 4 and 6 months p.i. As nigrostriatal degeneration is associated with deficits in these tests, one-tailed statistical tests were performed. In *Experiment 1* and *Experiment 2*, rats were assessed for activity in the open field and multiple gait parameters, respectively. Activity in the open field and gait parameters have been associated with inconsistent directionality in different PD models, therefore, for these measures, two-tailed statistical tests were used.

2.14.1. Cylinder test

Spontaneous forelimb use in the cylinder was conducted as described previously (Schallert, 2006; Paumier et al., 2015). Rats were placed in a transparent plexiglass cylinder (16.5 cm tall and 25 cm diameter), and video recorded under red light conditions. A mirror was positioned behind the cylinder to allow a view of all forelimb movements along the wall of the cylinder. Animals remained in the cylinder until at least 30 forelimb movements were made (approximately 2 min). A forelimb wall movement was counted when the rat made a weight-bearing forelimb placement on the wall of the cylinder while it was in an upright position on its hindlimbs. An investigator blind to experimental condition viewed the videos at half-speed and scored the first 20 left, right, or both forelimb wall placements. Results for each animal were recorded as percent of contralateral forelimb use and graphed by treatment group. Percentage of contralateral forelimb use for each rat was calculated using the formula: [(contra +1/2 both) divided by (ipsi + contra + both)] multiplied by 100%.

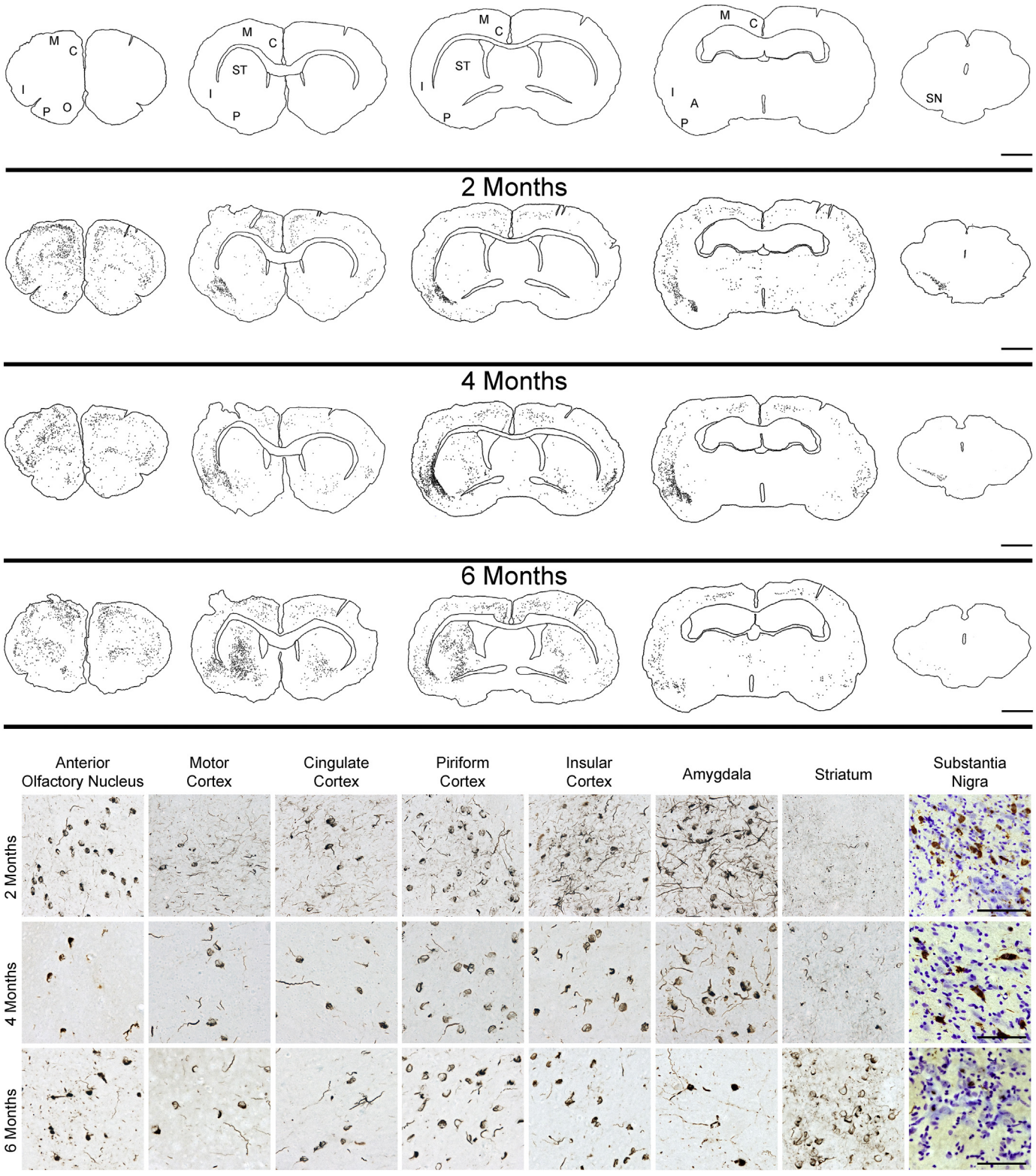

Fig. 3. Presence of pSyn pathology throughout brain regions which innervate the striatum. (Top) Traced and stippled images of representative sections throughout the rat brain from the 16 μg group at 2, 4, and 6-months post-injection (p.i.), as well as sections labeled for affected regions. Regions labeled are the anterior olfactory nucleus (O), motor cortex (M), cingulate cortex (C), piriform cortex (P), insular cortex (I), amygdala (A), striatum (ST), and substantia nigra (SN). Each dot represents a single phosphorylated α-syn at serine 129 (pSyn) staining cell in the section. Scale bar = 2 mm. **(Bottom)** Micrographs from regions with prevalent pSyn staining cells at 2, 4, and 6-months p.i. Scale bar = 100 μm.

2.14.2. Open field

Distance traveled in an open field was assessed using the ANY-maze video tracking system (Stoelting company). Rats were placed in an opaque 50 × 50 cm box with an open top for 30 min. Distance traveled in the first 5 min. Was measured and graphed as distance traveled/% baseline taken prior to surgeries. At the 6 month timepoint, control and 16 μg groups were administered a single 1 mg kg-1 intraperitoneal injection of amphetamine and recorded in the open field for 30 min. Under red light conditions.

2.14.3. Spontaneous activity/modified cylinder

Spontaneous activity was measured in a transparent plexiglass cylinder (25 cm diameter) placed on top of a clear plexiglass platform. A video camera oriented upwards was placed beneath the platform in order to be able to record forelimb and hindlimb steps. All rats were recored for 5 min under red light. An investigator blinded to treatment group viewed the videos at half or quarter speed depending on the degree of activity of the animal. Forelimb and hindlimb steps scored for each animal over a 2 min period, starting when all four paws were on the floor. A step was defined as the successive weight-bearing movement of left and right forelimbs or hindlimbs. Results from each animal were recorded and graphed by treatment group (Schallert et al., 2000; Fleming et al., 2004).

2.14.4. Adjusting step test

Rats were held with one forelimb restrained and the other placed on a treadmill belt. Treadmill speed was set at 6 m min^{-1}. Treadmill direction was based on the forelimb tested so that the forelimb would be moved towards the body (treadmill moved right for the left limb and left for the right limb). Two trials of at least 1 m were performed for each forelimb. A separate investigator viewed the videos at half-speed and measured the number of steps taken within 1 m (Olsson et al., 1995; Chang et al., 1999). The number of steps taken in the two trials were averaged for each side and served as the final score.

2.14.5. Gait analysis

A Noldus CatWalk XT system was used to assess 40 gait related variables (Table S1). Rats were allowed two trials, one per day, to acclimate to the catwalk system. The third day was considered the test trial and was analyzed for the experiment. The data for each rat was manually processed to designate the identity of each paw that touched the floor, and remove non-specific signal produced by other body parts (nose, tail, and testicles). Right and left forelimbs, and hindlimbs were grouped and plotted as separate data points grouped by treatment.

2.15. Statistics

Statistical analysis of data and graphing were performed using GraphPad Prism. Significance in all cases was set at $\alpha \leq 0.05$. Outliers were assessed using the absolute deviation from the median method (Leys et al., 2013), with a "very conservative" difference of 2.5× median absolute deviation used as the exclusion criteria. Additionally, samples injected with PFFs that lacked α-syn pathology were excluded as "missed injections". In total, there were four rats classified as missed injections, two from the 8 μg 2 month cohort, and two from the 8 μg 4 month cohort. There were five rats that died prior to the designated timepoint (three from the 16 μg 2 month cohort, one from the 8 μg 6 month cohort, and one from the 16 μg 6 month cohort). Groups of two were compared with a Student's *t*-test, groups of three or more were compared with a one-way ANOVA with a *post-hoc* Tukey test.

3. Results

3.1. Length of α-syn pre-formed fibrils

Monomeric α-syn, full length α-syn PFFs, and sonicated α-syn PFFs were imaged via transmission election microscopy to confirm ultrastructure prior to injection (Fig. S1A–C). Sonicated PFFs were measured to ensure that the increase in fibril concentration did not significantly alter the resulting fibril size. Fibril size distribution ranged from 13 to 132 nm for 2 μg μl^{-1}, and 5–181 nm for 4 μg μl^{-1} of total PFF (Fig. S1D). With 2 μg μl^{-1} of protein 88.1% of fibrils were < 60 nm and with 4 μg μl^{-1} 86.9% of fibrils were < 60 nm, in agreement with the previously identified optimal fibril length (Tarutani et al., 2016; Abdelmotilib et al., 2017). The average fibril sizes were 44.70 nm ± 0.43 at 2 μg μl^{-1} and 44.35 nm ± 0.39 at 4 μg μl^{-1} of PFF (Fig. S1E). There was no difference between mean total fibril sizes between groups (two-tailed *t*-test; $p = .5526$), indicating that the sonication parameters used were effective in both PFF concentration conditions and sufficient to induce pathology in vivo.

4. Temporal localization of phosphorylated α-syn (pSyn) inclusions throughout the brain

The location of pSyn immunoreactive inclusions throughout the brain at 2, 4 and 6 months p.i. was assessed (Fig. 3). Accumulation of pSyn was observed in the anterior olfactory nucleus, motor, cingulate, piriform, prelimbic, somatosensory, entorhinal, and insular cortices, amygdala, striatum, and SNpc. Qualitatively, pSyn inclusions in the anterior olfactory nucleus, motor and cingulate cortex, amygdala, and SNpc were most prevalent early, at the 2-month time point, and decreased overtime. Inclusions in the piriform, and insular cortex appeared to peak at 4 months, and then decrease by 6 months. Only in the striatum do inclusions of pSyn appear to increase over the course of the 6 month study. At 2 months, pSyn is not observed within cell soma of the striatum, but rather is present within neurites, presumably the terminals of innervating neurons that have seeded. After 4 months, and increasing further at 6 months, more soma-localized pSyn inclusions are present in the striatum.

5. Assessment of the nigrostriatal pathway

Examination of the SNpc was performed using antibodies to identify pSyn inclusions, oligomeric and fibrillar conformations of α-syn (O2), or fibrillar conformations specifically (F2, Vaikath et al., 2015). Neurodegeneration was assessed via TH immunoreactive (ir) and NeuNir neurons in the SNpc. The magnitude of striatal denervation was assessed by quantifying TH immunoreactivity within the striatum.

5.1. Neuropathology at 2 Months After Injection

5.1.1. Peak SNpc pSyn aggregate number, no loss of THir neurons, and PFF dose-dependent perturbations of striatal TH

At 2 months p.i., as expected, no inclusions were observed in the PBS injected control group or in the contralateral hemisphere of any PFF injected rat (Fig. S2). The ipsilateral hemisphere of 16 μg PFF group possessed over 2.5 fold more pSyn containing SNpc neurons (two-tailed *t*-test; $p = .0135$) than the 8 μg group (Fig. 4 A, B, G). The mean number of pSyn containing neurons in the 8 μg group was 1690 ± 603, and in the 16 μg group was 4712 ± 805. The mean of O2ir (stains α-syn oligomers and fibrils) neurons in the 8 μg group was 1562 ± 653, and 3019 ± 598 in the 16 μg group, with no significant difference between groups (two-tailed *t*-test; $p = .1382$) (Fig. 4 C, D, H). In contrast, we observed 3.5 fold more F2ir (stains α-syn fibrils only) neurons in the 16 μg group (two-tailed t-test; $p = .0142$) compared to the 8 μg group (Fig. 4 E, F, I). The mean of the F2ir neurons was 677 ± 429 at 8 μg, and in the 16 μg group was 2517 ± 312. Immunohistochemistry for total endogenous (non-phosphorylated) α-syn in the SNpc revealed dense inclusions only in the ipsilateral SNpc (Fig. S3). These inclusions were resistant to proteinase K digestion and also were thioflavin-S positive, demonstrating the presence of amyloid structures within the cells (Fig. S3). Based on immunofluorescence, pSyn is primarily present in

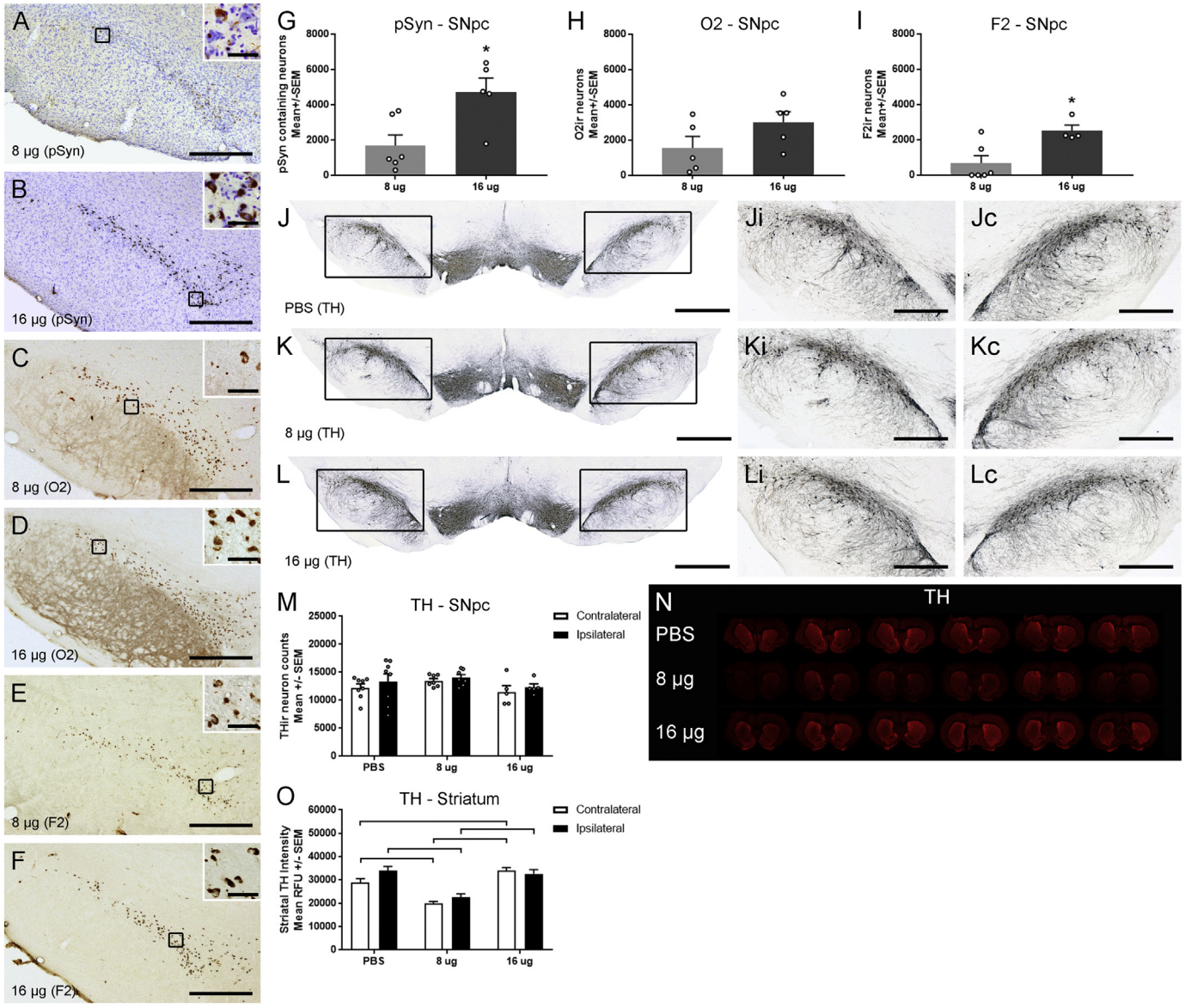

Fig. 4. Assessment of the nigrostriatal pathway at 2 months post-injection. Micrographs showing **(A, B)** phosphorylated alpha-synuclein (α-syn) at serine 129 (pSyn) with cresyl violet counterstain, **(C, D)** α-syn oligomers and fibrils (O2), and **(E, F)** α-syn fibrils (F2) immunohistochemistry (IHC) in the substantia nigra pars compacta (SNpc). **(A)** Ipsilateral SNpc from the 8 µg group stained for pSyn with a high magnification inset (boxed area). **(B)** Ipsilateral SNpc from the 16 µg group stained for pSyn with a high magnification inset (boxed area). **(C)** Ipsilateral SNpc from the 8 µg group stained for O2 with a high magnification inset (boxed area). **(D)** Ipsilateral SNpc from the 16 µg group stained for O2 with a high magnification inset (boxed area). **(E)** Ipsilateral SNpc from the 8 µg group stained for F2 with a high magnification inset (boxed area). **(F)** Ipsilateral SNpc from the 16 µg group stained for F2 with a high magnification inset (boxed area). **(G)** Total enumeration of pSyn containing neurons. **(H)** Total enumeration of O2 immunoreactive (O2ir) neurons. **(I)** Total enumeration of F2 immunoreactive (F2ir) neurons. **(J-L)** Tyrosine hydroxylase (TH) IHC in the SNpc. **(J)** phosphate buffered saline (PBS) control. Boxed areas are magnified to show the **(Ji)** ipsilateral and **(Jc)** contralateral SNpc. **(K)** 8 µg preformed fibrils (PFF). Boxed areas are magnified to show the **(Ki)** ipsilateral and **(Kc)** contralateral SNpc. **(L)** 16 µg PFF. Boxed areas are magnified to show the **(Li)** ipsilateral and **(Lc)** contralateral SNpc. **(M)** Stereological estimates of TH immunoreactive (THir) neurons in the SNpc. **(N)** Representative sections of TH immunofluorescence in the striatum. **(O)** Fluorescent densitometry of striatal TH (represented by sections in **(N)**). Columns indicate the group means, circles represent data points, error bars represent +1 standard error of the mean. Significant difference ($p \leq .05$) from respective control is denoted with a * or lines drawn over columns. Scale bar = 1000 µm in large **(J-L)**; 500 µm in **(A-F)**, **(Ji-Li)**, and **(Jc-Lc)**; and 50 µm in insets in **(A-F)**. (For interpretation of the references to colour in this figure legend, the reader is referred to the web version of this article.)

THir neurons, with a few exceptions of pSyn inclusions present in cells devoid of TH (Fig. S4). These exceptions are most likely dopamine neurons that have lost the TH phenotype, as in all cases, pSyn inclusions appear within, or in proximity to NeuNir cells (Fig. S4).

With regards to neurodegeneration, we observed no loss of SNpc THir neurons at 2 months (Fig. 4 J-L, M) in either of the PFF-injected treatment groups compared to PBS-injected controls. In the ipsilateral SNpc, the group means were 13,338 ± 1365 THir neurons in the control, 14,035 ± 530 in the 8 µg, and 12,344 ± 570 in the 16 µg group (one-way ANOVA; $p = .5787$). In the contralateral SNpc, the group means were 12,242 ± 668 THir neurons in the control, 13,487 ± 390 in the 8 µg, and 11,487 ± 1109 in the 16 µg group (one-way ANOVA; $p = .1809$).

In contrast to the SNpc where no PFF-induced differences in numbers of THir neurons were observed at 2 months, examination of TH relative fluorescent intensity within the striatum at this same time point revealed PFF-induced differences (Fig. 4 N, O). Specifically, TH immunoreactivity in the striatum was decreased bilaterally in the 8 µg PFF

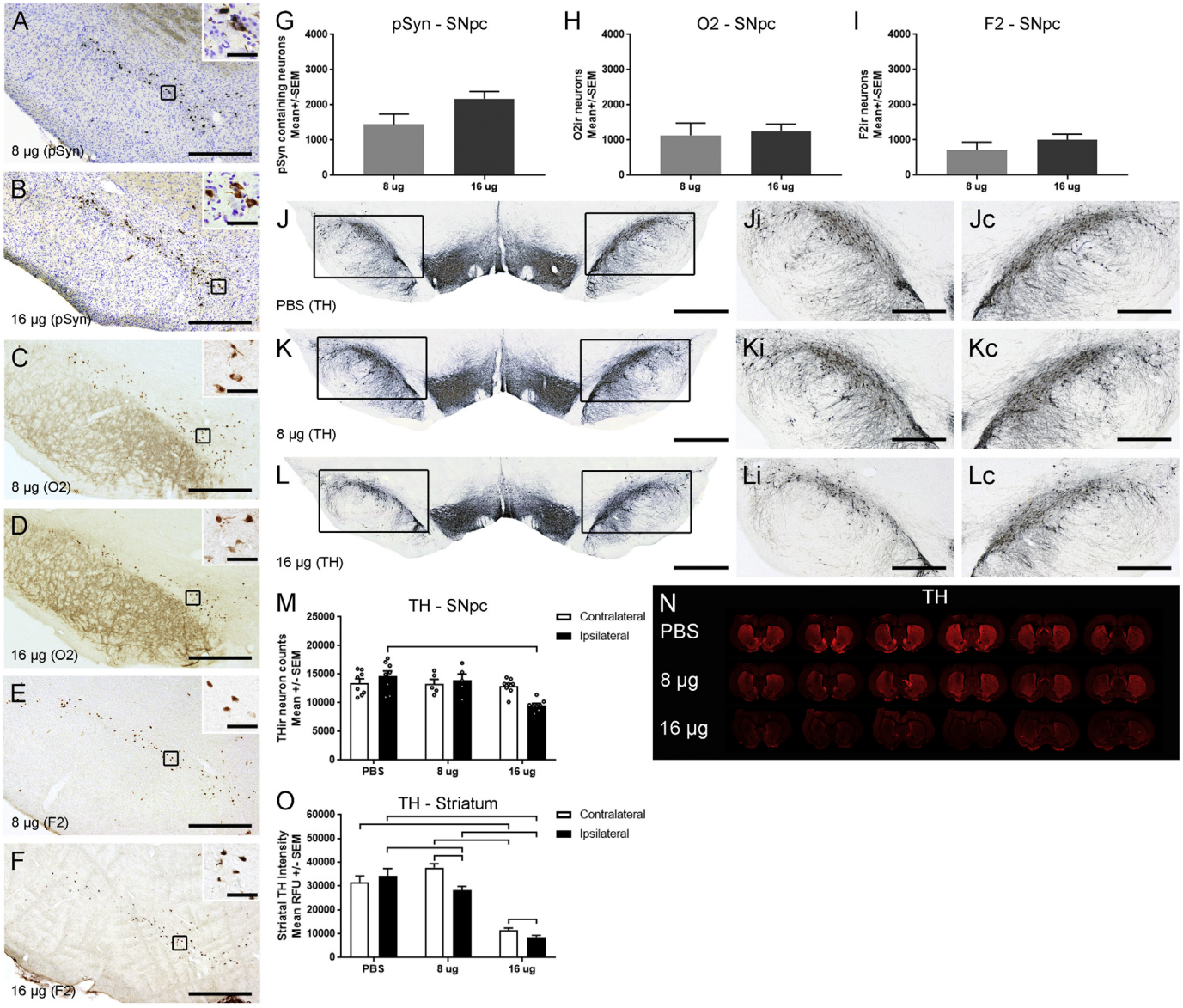

Fig. 5. Assessment of the nigrostriatal pathway at 4 months post-injection. Micrographs showing **(A, B)** phosphorylated alpha-synuclein (α-syn) at serine 129 (pSyn) with cresyl violet counterstain, **(C, D)** α-syn oligomers and fibrils (O2), and **(E, F)** α-syn fibrils (F2) immunohistochemistry (IHC) in the substantia nigra pars compacta (SNpc). **(A)** Ipsilateral SNpc from the 8 µg group stained for pSyn with a high magnification inset (boxed area). **(B)** Ipsilateral SNpc from the 16 µg group stained for pSyn with a high magnification inset (boxed area). **(C)** Ipsilateral SNpc from the 8 µg group stained for O2 with a high magnification inset (boxed area). **(D)** Ipsilateral SNpc from the 16 µg group stained for O2 with a high magnification inset (boxed area). **(E)** Ipsilateral SNpc from the 8 µg group stained for F2 with a high magnification inset (boxed area). **(F)** Ipsilateral SNpc from the 16 µg group stained for F2 with a high magnification inset (boxed area). **(G)** Total enumeration of pSyn containing neurons. **(H)** Total enumeration of O2 immunoreactive (O2ir) neurons. **(I)** Total enumeration of F2 immunoreactive (F2ir) neurons. **(J-L)** Tyrosine hydroxylase (TH) IHC in the SNpc. **(J)** phosphate buffered saline (PBS) control. Boxed areas are magnified to show the **(Ji)** ipsilateral and **(Jc)** contralateral SNpc. **(K)** 8 µg preformed fibrils (PFF). Boxed areas are magnified to show the **(Ki)** ipsilateral and **(Kc)** contralateral SNpc. **(L)** 16 µg PFF. Boxed areas are magnified to show the **(Li)** ipsilateral and **(Lc)** contralateral SNpc. **(M)** Stereological estimates of TH immunoreactive (THir) neurons in the SNpc. **(N)** Representative sections of TH immunofluorescence in the striatum. **(O)** Fluorescent densitometry of striatal TH (represented by sections in **(N)**). Columns indicate the group means, circles represent data points, error bars represent +1 standard error of the mean. Significant difference ($p \leq .05$) from respective control is denoted with a * or lines drawn over columns. Scale bar = 1000 µm in large **(J-L)**; 500 µm in **(A-F)**, **(Ji-Li)**, and **(Jc-Lc)**; and 50 µm in insets in **(A-F)**. (For interpretation of the references to colour in this figure legend, the reader is referred to the web version of this article.)

group compared to control (one-way ANOVA; $p < .0001$, Tukey test; $p = .0001$). Though no changes in TH immunoreactivity were observed in the ipsilateral striatum in the 16 µg PFF group compared to controls (Tukey test; $p = .8262$), there was a slight increase in the contralateral striatum (Tukey test; $p = .0240$).

5.1.2. Neuropathology at 4 months after injection

5.1.2.1. Reduced SNpc pSyn aggregate number, ipsilateral THir neuron loss, PFF dose-dependent perturbations of striatal TH. At 4 months p.i., the previously observed dose-dependent differences in inclusion formation in the SNpc were no longer observed, with no significant differences in number of pSynir, O2ir, or F2ir SNpc neurons between the 8 and 16 µg PFF groups. The mean of pSyn containing neurons in the 8 µg group was 1442 ± 300, and in the 16 µg group was 2174 ± 208 (two-tailed *t*-test; $p = .0602$) (Fig. 5 A, B, G). The mean number of O2ir neurons in the 8 µg group was 1137 ± 346, was 1256 ± 203 in the 16 µg group (two-tailed t-test; $p = .7580$) (Fig. 5 C, D, H). The mean of F2ir neurons was 716 ± 224 at 8 µg, and in the 16 µg group was 1004 ± 163 (two-

tailed t-test; $p = .3070$) (Fig. 5 E, F, I).

Examination of the number of SNpc THir neurons revealed a significant decrease in ipsilateral THir neurons compared to control, but only in the ipsilateral hemisphere of the 16 μg PFF group (one-way ANOVA; $p = .0008$, Tukey test; $p = .0006$) (Fig. 5 J-L, M). In the ipsilateral SNpc, the group means of THir neurons were 14,636 ± 920 for the control, 12,798 ± 1066 in the 8 μg, and 9562 ± 347 in the 16 μg group. There was no loss of THir neurons in the contralateral SNpc at 4 months (one-way ANOVA; $p = .2259$). In the contralateral SNpc, the group means were 13,461 ± 732 for the control, 13,360 ± 562 in the 8 μg, and 12,929 ± 475 in the 16 μg group. To determine whether ipsilateral THir neuron loss in the 16 μg group represented phenotype vs. neuronal loss, total neurons within the SNpc were quantified using immunohistochemistry for NeuN. There was no difference in NeuNir neurons between the ipsilateral SNpc hemispheres of 16 μg PFF-injected and PBS control rats (two-tailed *t*-test; $p = .4090$) (Fig. S5 A-C). Group means were 25,945 ± 1757 for the control and for the 27,922 ± 2323 16 μg group. These results suggest the loss of ipsilateral THir SNpc neurons in the 16 μg PFF rats observed at 4 months reflects loss of TH phenotype.

TH immunoreactivity in the ipsilateral striatum was decreased in the 8 μg group compared to control (one-way ANOVA; $p < .0001$, Tukey test; $p = .0428$) with no change in the contralateral striatal hemisphere observed (Tukey test; $p = .4851$). (Fig. 5 N, O). Additionally, in rats injected with 16 μg of PFFs, a bilateral decrease in TH immunoreactivity was observed compared to both the controls (one-way ANOVA; Tukey test; $p < .0001$) and the 8 μg group (Tukey test; $p < .0001$). Comparing ipsilateral to contralateral hemispheres, there was no difference in TH in the control group (two-tailed *t*-test; $p = .4915$), however, TH was higher contralaterally in the 8 μg (two-tailed *t*-test; $p = .0009$) and 16 μg groups (two-tailed t-test; $p = .0059$).

5.1.3. Neuropathology at 6 months after injection

5.1.3.1. Minimal pSyn aggregate number in the SNpc, bilateral THir neuron loss, bilateral loss of PFF dose-related striatal TH. In the 6-month cohort, an α-syn monomer (16 μg total) group was included as an additional control. All α-syn treatment groups possessed pSyn containing neurons in the SNpc. The 16 μg and 8 μg PFF groups displayed fewer pSyn containing neurons than earlier time points, with no difference between the 8 and 16 μg groups (Tukey test; $p = .7193$). The monomer group possessed significantly fewer pSyn containing neurons than the 8 or 16 μg PFF group (one-way ANOVA; $p < .0001$, Tukey test; $p < .0001$) (Fig. 6 A-B, G; Fig. S6 A, D). There were 42 ± 9 pSyn SNpc neurons in the monomer control, 673 ± 91 in the 8 μg PFF group and 599 ± 76 in the 16 μg of PFF group. Similarly, the monomer group displayed fewer O2ir neurons than the 8 and 16 μg groups (one-way ANOVA; $p < .0107$, Tukey test; $p < .03$) (Fig. 6 C-D, H; Fig. S6 B, E), with no difference in O2ir neurons between the 8 and 16 μg PFF groups (Tukey test; $p = .9907$). The mean of the O2ir neurons was 46 ± 25 in the monomer control, 220 ± 31 in the 8 μg PFF group and 212 ± 65 in the16 μg PFF group. No F2ir neurons were observed in the monomer control group (Fig. 6 *E*-F, I; Fig. S6 C, F) and no differences were observed in F2ir neurons between the 8 and 16 μg groups (Tukey test; $p = .9261$). The mean number of F2ir neurons in the 8 μg PFF group was 206 ± 37, and 229 ± 64 in the 16 μg PFF group.

Quantitation of THir neurons in the SNpc revealed no significant differences between PBS and monomer controls at 6 months after injection in either the ipsilateral (two-way t-test; $p = .4422$) or contralateral (two-way t-test; $p = .9880$) hemispheres, thus, the PBS and monomer control group were grouped together for subsequent statistical analysis. In the ipsilateral SNpc, there was a decrease in THir neurons in both the 8 μg PFF (one-way ANOVA; $p < .0001$, Tukey test, $p < .0001$) and 16 μg PFF groups (Tukey test, $p < .0001$) compared to controls (Fig. 6 J-L, M; Fig. S6 G-H). Additionally, the 16 μg PFF group possessed fewer ipsilateral THir neurons than the 8 μg group (Tukey test, $p = .0305$). Compared to controls, the 8 μg PFF group had a ~28% loss and the 16 μg PFF a ~48% loss of THir neurons in the ipsilateral SNpc. In the ipsilateral SNpc, the group means were 13,797 ± 773 SNpc THir neurons in the PBS controls, 14,655 ± 772 for monomer, 9907 ± 687 in the 8 μg PFF group, and 7223 ± 457 in the 16 μg PFF group. On the contralateral side, there was a decrease in THir neurons in both the 8 (one-way ANOVA; $p = .0005$, Tukey test, $p = .0223$) and 16 μg PFF groups (Tukey test, $p = .0008$) compared to controls. Additionally, the magnitude of THir SNpc neuron loss in the contralateral hemisphere was identical between the 8 and 16 μg PFF groups (Tukey test, $p = .5390$). Compared to controls, the 8 μg PFF group possessed ~17% fewer and the 16 μg PFF group possessed ~24% fewer THir neurons in the contralateral SNpc. In the contralateral SNpc the group means were 14,258 ± 646 for the PBS control, 14,244 ± 620 for monomer, 11,857 ± 729 in the 8 μg PFF group, and 10,780 ± 825 in the 16 μg PFF group. Comparing ipsilateral to contralateral hemispheres, there was no difference in THir neurons in the PBS (two-tailed *t*-test; $p = .6526$), monomer (two-tailed t-test; $p = .6830$), PBS and monomer combined (two-tailed *t*-test; $p = .9715$) or 8 μg PFF groups (two-tailed t-test; $p = .0694$), although there was a greater degree of loss ipsilaterally in the 16 μg PFF group (two-tailed *t*-test; $p = .0017$). Additionally, the degree of contralateral loss of THir neurons correlated with the extent of ipsilateral THir loss (Pearson correlation; $r = 0.7421$; $p < .0001$) (Fig. 6 P). To distinguish between neuronal loss and loss of TH phenotype, stereological assessment of SNpc NeuNir neurons was performed. On the ipsilateral side, we observed a decrease in NeuNir neurons in both the 8 (one-way ANOVA; $p < .0001$, Tukey test, $p < .0001$) and 16 μg PFF groups (Tukey test, $p = .0006$) compared to controls (Fig. S5 D-G). No differences in ipsilateral NeuNir SNpc were observed between the 8 and 16 PFF μg groups (Tukey test, $p = .6890$). In the ipsilateral SNpc, the group means were 31,603 ± 1543 for the PBS control, 28,677 ± 1268 for monomer group, 21,327 ± 826 in the 8 μg PFF group, and 22,970 ± 1710 in the 16 μg PFF group. On the contralateral side, a decrease in SNpc NeuNir neurons was observed in both the 8 (one-way ANOVA; $p = .0011$, Tukey test, $p = .0089$) and 16 μg PFF groups (Tukey test, $p = .0038$) compared to controls, with no difference observed between the 8 and 16 μg PFF groups (Tukey test, $p = .9579$). In the contralateral SNpc, the group means were 28,809 ± 1298 for the PBS controls, 29,276 ± 1016 for the monomer groups, 23,786 ± 1375 in the 8 μg PFF group, and 23,251 ± 1710 in the 16 μg PFF group. As with THir SNpc neurons, the degree of contralateral loss of NeuNir neurons correlated with the extent of ipsilateral NeuNir loss (Pearson correlation; $r = 0.7417$; $p < .0001$) (Fig. S5 H). Collectively, these results suggest that the greater magnitude of ipsilateral THir neuron loss associated with injection of a larger quantity of α-syn PFFs represents a loss of TH phenotype rather than a greater magnitude of overt degeneration.

Examination of TH immunoreactivity in the striatum revealed a bilateral decrease in both the 8 and 16 μg PFF groups compared to controls (one-way ANOVA; $p < .0001$, Tukey test; $p \leq .0007$) (Fig. 6 N, O) with the 16 μg PFF group exhibiting decreased TH immunoreactivity compared to the 8 μg PFF group (Tukey test; $p = .0007$). Comparing ipsilateral to contralateral hemispheres, there was no difference in TH immunoreactivity in the PBS group (two-tailed *t*-test; $p = .0702$), however, in both the 8 and 16 μg PFF group TH immunoreactivity was decreased in the ipsilateral striatum compared to the contralateral striatum (two-tailed t-test; $p \leq .0121$).

5.1.4. Sensorimotor assessment

Due to the greater magnitude of nigral THir neuron loss and striatal denervation in the 16 μg PFF group we focused on statistical comparisons between this treatment and controls. The 6 month cohorts of PBS and 16 μg PFF rats were assessed for motor deficits at 2, 4, and 6 months following intrastriatal injection. Distance traveled in the open field was not affected by PFF injections at any time point (Fig. S7 *E*-F). Specifically, comparing control rats to the 16 μg PFF group revealed no difference in distance traveled either after saline (two-tailed *t*-test;

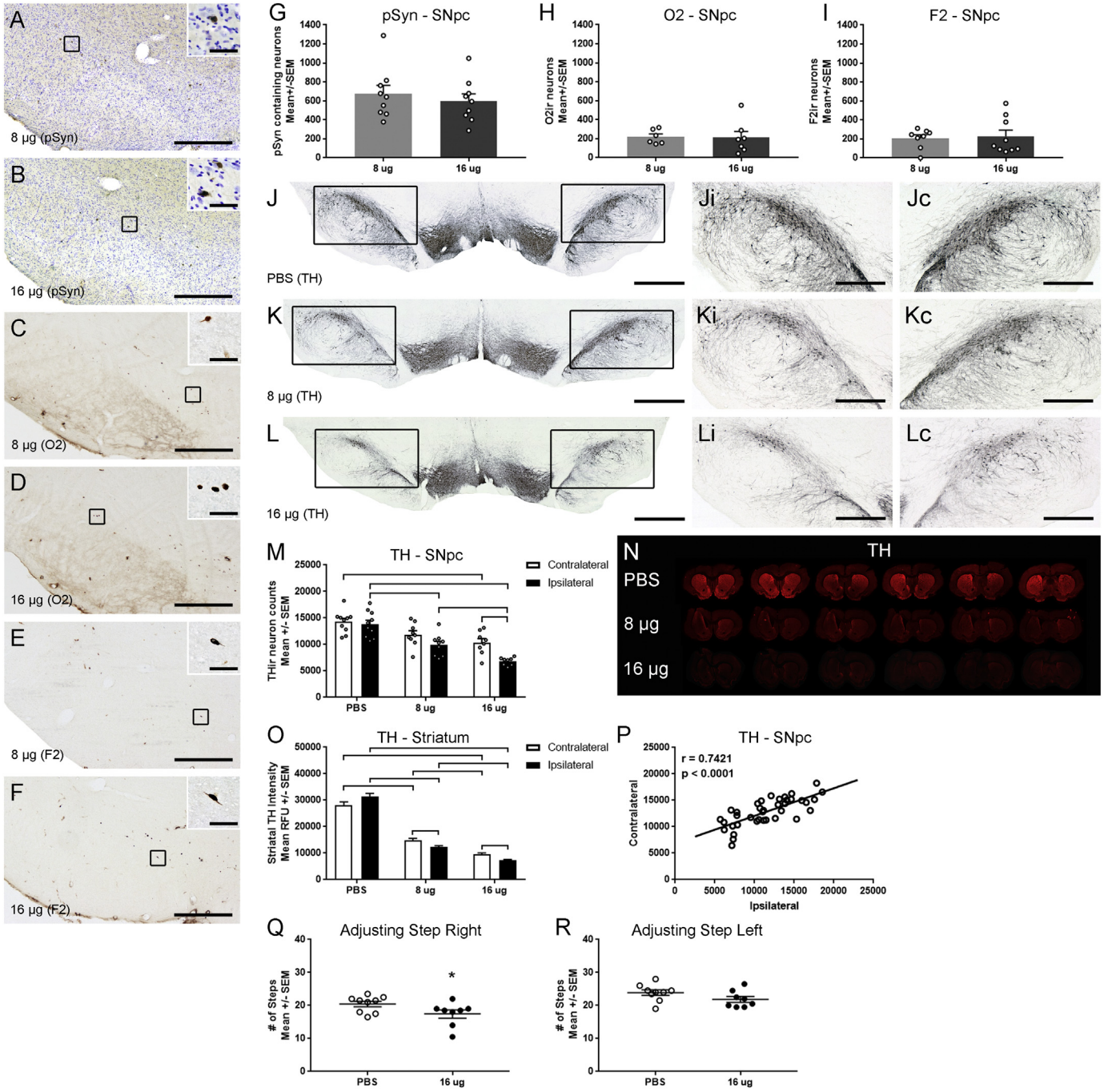

Fig. 6. Assessment of the nigrostriatal pathway at 6 months post-injection.
Micrographs showing **(A, B)** phosphorylated alpha-synuclein (α-syn) at serine 129 (pSyn) with cresyl violet counterstain, **(C, D)** α-syn oligomers and fibrils (O2), and **(E, F)** α-syn fibrils (F2) immunohistochemistry (IHC) in the substantia nigra pars compacta (SNpc). **(A)** Ipsilateral SNpc from the 8 µg group stained for pSyn with a high magnification inset (boxed area). **(B)** Ipsilateral SNpc from the 16 µg group stained for pSyn with a high magnification inset (boxed area). **(C)** Ipsilateral SNpc from the 8 µg group stained for O2 with a high magnification inset (boxed area). **(D)** Ipsilateral SNpc from the 16 µg group stained for O2 with a high magnification inset (boxed area). **(E)** Ipsilateral SNpc from the 8 µg group stained for F2 with a high magnification inset (boxed area). **(F)** Ipsilateral SNpc from the 16 µg group stained for F2 with a high magnification inset (boxed area). **(G)** Total enumeration of pSyn containing neurons. **(H)** Total enumeration of O2 immunoreactive (O2ir) neurons. **(I)** Total enumeration of F2 immunoreactive (F2ir) neurons. **(J-L)** Tyrosine hydroxylase (TH) IHC in the SNpc. **(J)** phosphate buffered saline (PBS) control. Boxed areas are magnified to show the **(Ji)** ipsilateral and **(Jc)** contralateral SNpc. **(K)** 8 µg preformed fibrils (PFF). Boxed areas are magnified to show the **(Ki)** ipsilateral and **(Kc)** contralateral SNpc. **(L)** 16 µg PFF. Boxed areas are magnified to show the **(Li)** ipsilateral and **(Lc)** contralateral SNpc. **(M)** Stereological estimates of TH immunoreactive (THir) neurons in the SNpc. **(N)** Representative sections of TH immunofluorescence in the striatum. **(O)** Fluorescent densitometry of striatal TH (represented by sections in **(N)**). **(P)** Pearson correlation plots for contralateral vs ipsilateral TH. **(Q)** Right forelimb adjusting step. **(R)** Left forelimb adjusting step. Columns indicate the group means, circles represent data points, error bars represent +1 standard error of the mean. Significant difference ($p \leq .05$) from respective control is denoted with a * or lines drawn over columns. Scale bar = 1000 µm in large **(J-L)**; 500 µm in **(A-F)**, **(Ji-Li)**, and **(Jc-Lc)**; and 50 µm in insets in **(A-F)**. (For interpretation of the references to colour in this figure legend, the reader is referred to the web version of this article.)

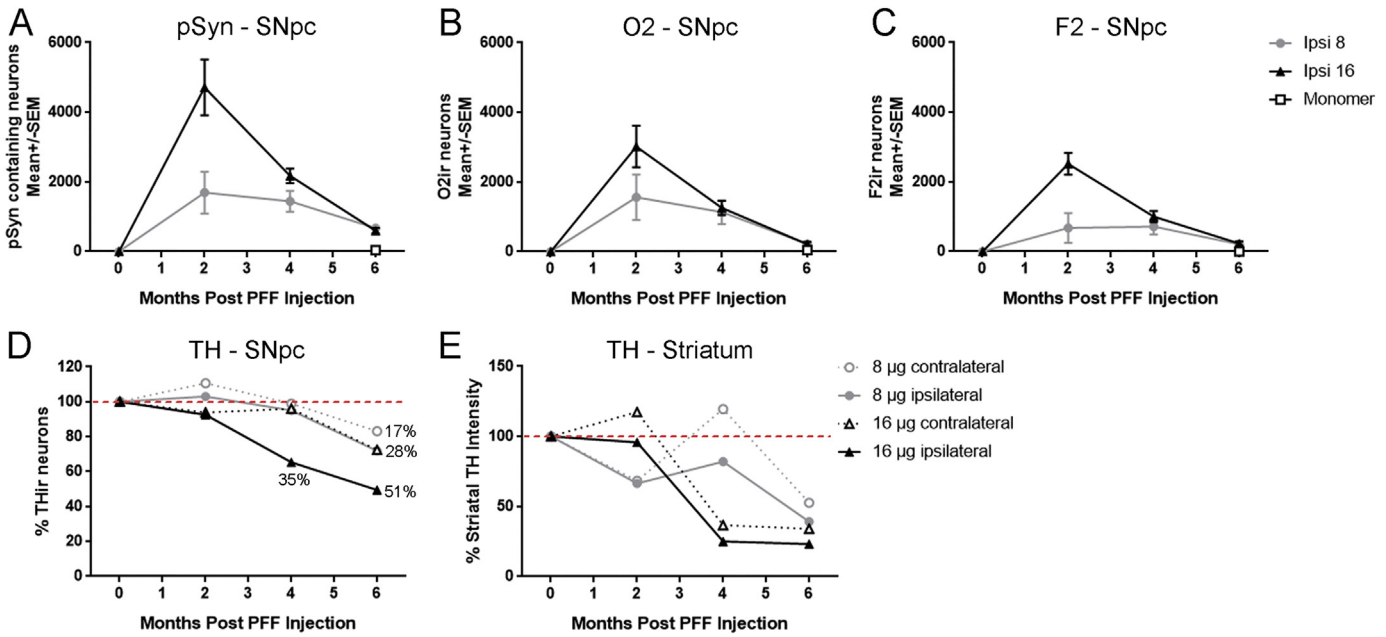

Fig. 7. Temporal progression within the PFF model. Total enumeration at 2, 4 and 6 months of **(A)** phosphorylated alpha-synuclein (α-syn) at serine 129 (pSyn), **(B)** α-syn oligomers and fibrils (O2), and **(C)** α-syn fibrils (F2) immunoreactive (F2ir) neurons in the monomer, 8 and 16 µg groups. **(D)** Percent loss of tyrosine hydroxylase immunoreactive (THir) neurons in the ipsilateral and contralateral SNpc in the 8 and 16 µg groups. Fluctuations in striatal **(E)** TH. Symbols indicate the group means, error bars represent ± 1 standard error of the mean.

$p = .4290$) or after amphetamine injection (two-tailed *t*-test; $p = .4128$) when tested at 6 months (Fig. S7 G).

Spontaneous activity in the cylinder was used to assess forelimb and hindlimb stepping (Fig. S7 C, D). No deficits in forelimb or hindlimb use were observed at any time point. Specifically, at 6 months there was no difference in forelimb (one-tailed *t*-test; $p = .3311$) or hindlimb (one-tailed t-test; $p = .3556$) stepping between the control and 16 µg PFF group.

To assess postural stability, a modified version of the adjusting step test was used. At the 6-month time point no differences were observed between rats injected with 16 µg PFFs compared to PBS-injected rats in use of the ipsilateral forelimb (one-tailed t-test; $p = .0622$). In contrast, rats injected with 16 µg PFFs displayed decreased use of the contralateral forelimb (one-tailed t-test; $p = .0292$) (Fig. 6 Q, R).

Lastly, no forelimb use asymmetry was detected in the cylinder at 6 months between the control and 16 µg group (one-tailed t-test; $p = .1264$) or at any earlier time points (Fig. S7 E).

5.2. Longitudinal pathological changes associated with unilateral PFF injections

Neuropathological changes associated with intrastriatal α-syn PFF injection followed a distinct pattern with slight temporal shifts and magnitude of effects impacted by the quantity of PFFs injected. Intraneuronal inclusions in the SNpc peaked at 2 months and tapered off by 6 months (Fig. 7 A, B, C). This peak was more readily apparent in the higher quantity 16 µg PFF group than the 8 µg PFF group.

Ipsilateral loss of SNpc THir neurons (Fig. 7 D) is first evident at 4 months after PFF injection, however, the magnitude of loss was only significant when the higher quantity of PFFs was injected. In both PFF-injected groups, ipsilateral THir neuron degeneration continues after 4 months resulting in further nigral neuron loss by 6 months. With regards to the contralateral nigral hemisphere, injection of the higher quantity 16 µg PFF group reveals that ipsilateral THir neuron loss precedes contralateral THir neuron loss and overt nigral cell loss.

In the striatum, we observed dynamic changes in TH immunoreactivity over time that were distinctly impacted by PFF quantity (Fig. 7 E). With 16 µg PFF injections TH immunoreactivity in the striatum appeared to be maintained or upregulated up to 2 months, respectively, followed by severe loss by 4 months that was maintained at 6 months. In the 8 µg PFF group this TH immunoreactivity maintenance/upregulation was delayed with ultimately the same severe loss observed at 6 months. In both PFF treatment conditions these striatal changes in TH immunoreactivity occurred bilaterally with the ipsilateral striatum ultimately appearing slightly more depleted at the 6-month time point.

5.3. Effects of bilateral Intrastriatal PFF injections

Unilateral PFF injections in both the 8 and 16 µg PFF groups led to neurodegeneration in both nigrostriatal hemispheres by 6 months p.i., despite the absence of pSyn containing neurons in the contralateral SNpc. The smaller magnitude loss observed on the contralateral side suggested that the magnitude of symmetric nigrostriatal degeneration may be further augmented via bilateral PFF injections. Therefore, an additional experiment in which bilateral intrastriatal injections of PFFs (total of 32 µg PFF, 16 µg per striatum) or an equal volume of PBS was performed. All rats were examined for neuropathology at 6 months and assessed for motor impairments at baseline and 2, 4 or 6 months (Fig. 8).

At the 6-month time point total enumeration of pSyn containing neurons in the SNpc revealed 848 ± 63 pSynir neurons on the left side and 904 ± 59 on the right side, with no difference between hemispheres (two-tailed *t*-test; $p = .5526$) (Fig. 8 A-B). The mean number of THir neurons in the left SNpc was 16,436 ± 436 in PBS and decreased to 7591 ± 492 in PFF injected animals (two-tailed t-test; $p < .0001$). In the right SNpc, the mean number of THir neurons was 15,438 ± 771 in PBS injected rats compared to 7981 ± 522 in PFF injected animals, representing a significant decrease (two-tailed t-test; $p < .0001$). Total THir neurons in both SNpc were 31,874 ± 1011 in PBS and 15,572 ± 894 in PFF injected animals (two-tailed t-test; $p < .0001$) (Fig. 8 C-E). In summary, rats injected bilaterally with PFFs had an average loss of approximately 50% of THir neurons in both hemispheres. In addition, PBS controls from all timepoints of the unilaterally

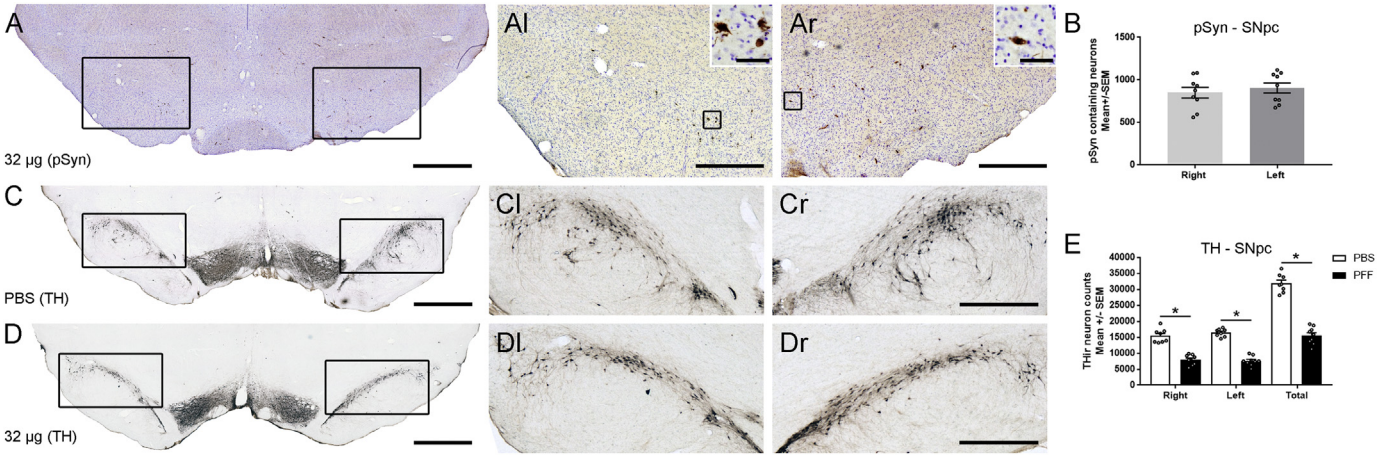

Fig. 8. Effects of bilateral PFF injections on pSyn, neurodegeneration, and motor behaviors at 6 months. Representative micrograph of **(A)** phosphorylated alpha-synuclein (α-syn) at serine 129 (pSyn) with cresyl violet counterstain in the 32 µg preformed fibril (PFF) group, showing the **(Al)** left and **(Ar)** right substantia nigra pars compacta (SNpc) with high magnification inset (boxed area). **(B)** Total enumeration of pSyn containing neurons in the left and right SNpc. **(C-D)** Tyrosine hydroxylase (TH) immunohistochemistry (IHC) in the SNpc. **(C)** Phosphate buffered saline (PBS) control. Boxed areas are magnified to show the **(Cl)** left and **(Cr)** right SNpc. **(D)** 32 µg PFF group. Boxed areas are magnified to show the **(Dl)** left and **(Dr)** right SNpc. **(E)** Stereological estimates of TH immunoreactive (THir) neurons in the left, right, and both SNpc. Columns indicate the group means, circles represent data points, error bars represent +1 standard error of the mean. Significant difference ($p \leq .05$) from respective control is denoted with a *. Scale bar = 1000 µm in large **(A)**, **(C-D)**; 500 µm in **(Al)**, **(Cl-Dl)**, **(Ar)**, **(Cr-Dr)**; and 50 µm in insets in **(Al)**, **(Cl-Dl)**, **(Ar)**, **(Cr-Dr)**. (For interpretation of the references to colour in this figure legend, the reader is referred to the web version of this article.)

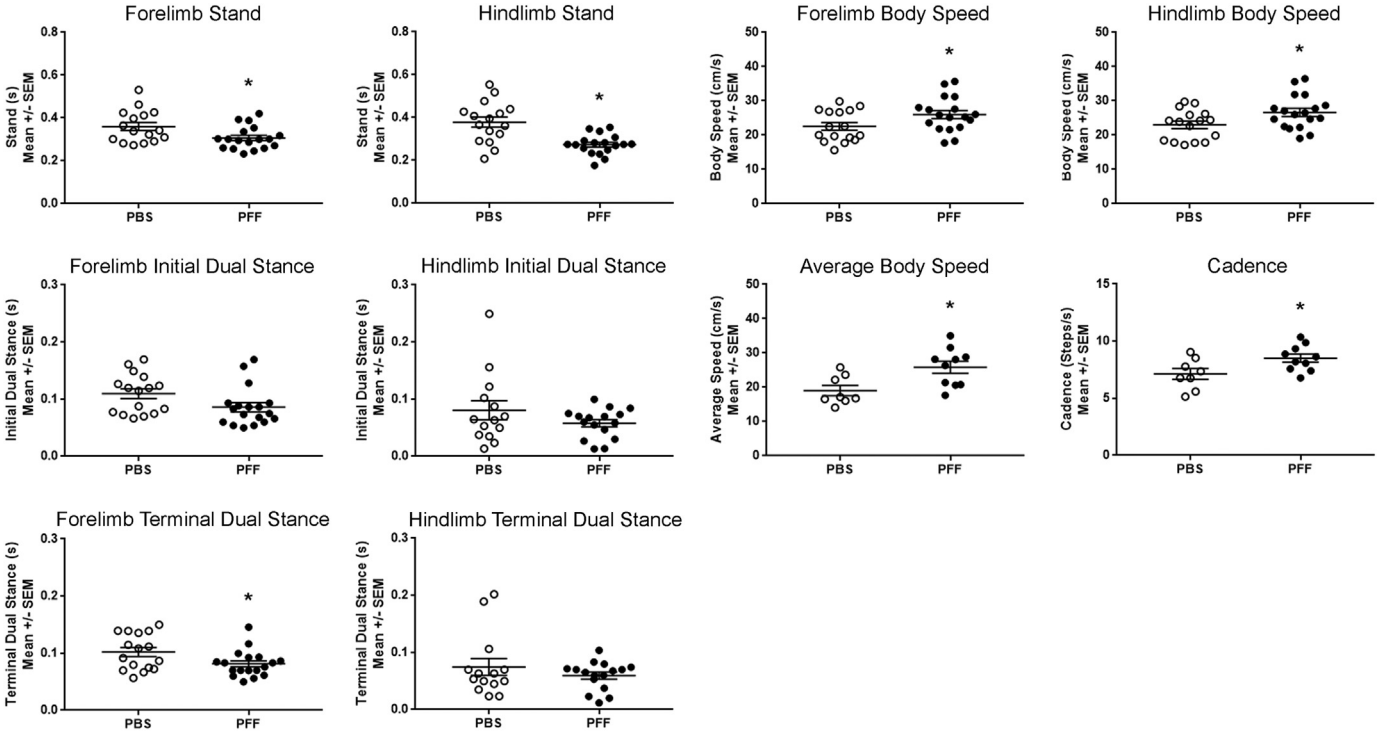

Fig. 9. Effects of bilateral PFF injections on motor behaviors at 6 months. Motor assessment for forelimb and hindlimb catwalk results for stand, initial dual stance, terminal dual stance, body speed, and animal averaged results for body speed, and step cadence. Symbols represent each limb/paw or animal in the case of body speed and cadence, with group means and error bars representing ± 1 standard error of the mean.

injected rats were compared with the bilateral rats. There was no difference in THir neurons in the injected hemisphere between groups (one-way ANOVA; $p = .1293$) or the uninjected hemisphere between groups (one-way ANOVA; $p = .1281$) (Fig. S8).

To further examine motor behaviors in bilaterally injected rats, the CatWalk automated gait analysis system was used to simultaneously analyze up to 40 different gait metrics. Of these parameters, we found stand time (duration of contact between paw and floor), terminal dual stance time (duration where both fore or hindlimbs are in contact with the floor at the end of a step cycle), body speed (speed of fore and hindlimbs over the run), average body speed (speed of the entire body over a run), and cadence (steps per second) were affected in either the fore or hindlimb (Fig. 9). In forelimb stand time, the PBS group had an average of 0.3599 ± 0.0189 s, whereas the PFF group had a decreased stand time of 0.3066 ± 0.0126 s (two-tailed t-test, $p = .0226$). In hindlimb stand time, the PBS group had an average of 0.3786 ± 0.0240 s, whereas the PFF group had a decreased stand time of 0.2735 ± 0.0109 s (two-tailed t-test, $p = .0002$). In forelimb

terminal dual stance time, the PBS group had an average of 0.1022 ± 0.0078 s, whereas the PFF group had a decreased stand time of 0.0815 ± 0.0054 s (two-tailed t-test, $p = .0342$). Similarly, initial dual stance time for forelimb showed a strong trend towards a decrease in the PFF treatment group ($p = .0509$). In the hindlimb terminal dual stance, the PBS group had an average of 0.0745 ± 0.0148 s, whereas the PFF group had a decreased stand time of 0.0593 ± 0.0062 s (two-tailed t-test, $p = .3333$). In forelimb body speed, the PBS group had an average of 0.3599 ± 0.0189 cm/s, whereas the PFF group displayed an increased rate of 0.3066 ± 0.0126 cm/s (two-tailed t-test, p = .0226). In hindlimb body speed, the PBS group had an average of 23.00 ± 1.09 s, whereas the PFF group had an increased rate of 26.64 ± 1.16 cm/s (two-tailed t-test, $p = .0299$). As for average speed, the PBS group had an average of 19.03 ± 1.50 cm/s, whereas the PFF group had an increased rate of 25.84 ± 1.76 cm/s (two-tailed t-test, $p = .0113$). The overall step cadence for the PBS group had an average of 7.1260 ± 0.476 steps/s, whereas the PFF group had an increased rate of 8.507 ± 0.356 steps/s (two-tailed t-test, $p = .0305$). Other results related to these metrics are graphed in Fig. S9, while all results and statistics are found in the supplementary dataset. Collectively, metrics from the CatWalk system suggest decreased standing time, increased speed and increased cadence in rats receiving bilateral PFF injections.

6. Discussion

In this study, we show the bilateral effects elicited by increasing the amount of α-syn PFFs unilaterally injected into the dorsal striatum. Injection of increasing quantity of α-syn PFFs leads to increased pSyn, O2, and F2ir inclusions within the SNpc, and exacerbates the degree of subsequent neurodegeneration of nigral dopamine neurons. Examining temporal events related to neurodegeneration, we observed ipsilateral loss of TH phenotype occurs before contralateral phenotype loss as well as bilateral neurodegeneration, suggesting that ipsilateral degeneration precedes and potentially contributes to contralateral degeneration.

Additionally, a temporal shift in the striatum is observed. Specifically, early compensatory increases in striatal TH immunoreactivity precede eventual loss. This increase appears accelerated by increased inclusion burden. Maximal loss of TH immunoreactivity occurs in the 16 μg PFF group prior to maximal loss of SNpc soma, suggesting axonopathy precedes cell body degeneration, similar to early PD (Kordower et al., 2013). It is important to note that measures of striatal TH immunoreactivity do not necessarily reflect total changes in protein or detect axonopathy. Further studies examining how PFF-triggered neurodegeneration impacts the functionality of nigrostriatal dopaminergic terminals should be performed in the future.

The site of fibril injection influences the location where pSyn positive inclusions develop within the brain. The anterior olfactory nucleus, motor, cingulate, piriform, prelimbic, somatosensory, entorhinal, and insular cortices, amygdala, striatum, and SNpc, all regions shown to contain inclusions in previous studies (Luk et al., 2012; Luk et al., 2016; Paumier et al., 2015; Duffy et al., 2018b). Neurons within these regions directly innervate the striatum (Wall et al., 2013) and the results do not support additional spread or second order propagation of pathological α-syn. In the striatum, the presence of pSyn immunoreactivity appears to peak at 6 months. It is still unclear why there is a delay in inclusion formation in the striatum, which requires more investigation in the future. With the exception of the striatum, all regions showed an eventual decrease in inclusion bearing cells by 6 months. The exact cause of this apparent decrease in inclusions in regions other than the SNpc is not entirely clear. It is possible, that like the SNpc, neurodegeneration occurs within these regions. A previous report documenting the loss of dendritic spines on layer V neurons within somatosensory cortex after intrastriatal PFF injection supports the concept that cortical inclusions are associated with a cytotoxic phenotype (Blumenstock et al., 2017). Alternatively, it is possible that pSyn is being degraded and is no longer detectable by the epitope used that recognizes full length pSyn. The autophagic degradation of full length pSyn can produce a toxic form of pSyn, referred to as pSyn* or pSyn STAR (α-syn truncated adamant and reactive) pSyn*, which lacks N and C terminal ends and is mitotoxic (Grassi et al., 2018, 2019). A transition from pSyn to pSyn* may also explain why the number of inclusion containing neurons, detected with an epitope against full length pSyn, decreases within the SNpc prior to neurodegeneration. As such, future studies should examine potential neurodegeneration within the amygdala and cortical regions, as well as a temporal examination of pSyn* in relation to pSyn."

By injecting more PFFs at optimized coordinates, we observe more than double the number of inclusion-containing neurons than what we previously observed at the peak of aggregation (Paumier et al., 2015; Duffy et al., 2018b). Likewise, the greater number of inclusions within the ipsilateral hemisphere is associated with a more rapid and pronounced degeneration within the ipsilateral hemisphere. There was no degeneration associated with the monomer control, however a few inclusion-containing neurons were apparent at 6 months. The number of monomer-triggered inclusions is dwarfed by those found in both PFF groups, however. We previously also have observed modest inclusion formation at 6 months following intrastriatal monomer injection to rats (Paumier et al., 2015), whereas other studies in mice or using intranigral injections in rats have not detected the formation of inclusions (Volpicelli-Daley et al., 2011; Luk et al., 2012; Abdelmotilib et al., 2017). In our current study, the monomers were not subjected to additional centrifugation prior to use in order to remove any pelletable material that could have formed (Polinski et al., 2018). It is possible that the omission of centrifugation could have lead to the formation of the inclusions. At the comparable 6-month time point, the ipsilateral loss of 48% of THir neurons is greater than the 35–40% loss previously reported with intrastriatal PFF injections (Paumier et al., 2015; Duffy et al., 2018b). Significant ipsilateral TH phenotype loss occurs at least one month earlier than shown previously and prior to contralateral loss, confirming that contralateral degeneration occurs after a threshold of ipsilateral neurodegeneration has been met (Duffy et al., 2018b). It is possible that some loss of the TH phenotype in the SNpc occurs earlier than 4 months, and is masked by signal amplification in immunohistochemistry.

One of the most surprising, yet consistent findings that we have observed in the rat α-syn PFF model is that unilateral injections of PFFs induce formation of ipsilateral SNpc inclusions, result in bilateral degeneration of nigral neurons. We have previously observed this phenomenon following unilateral intrastriatal injections in two independent studies (Paumier et al., 2015; Duffy et al., 2018b) however, we note that this same phenomenon has not been observed following intrastriatal PFF injections to mice (Luk et al., 2012; Luk et al., 2016). Our present findings pinpoint the exact timing when contralateral degeneration occurs relative to ipsilateral degeneration. Ipsilateral degeneration is observed first at 4 months, and is followed by appreciable contralateral degeneration at 6 months. This observation of "inclusion-independent" contralateral degeneration suggests an additional pathophysiological mechanism impacting the contralateral hemisphere. Neuroinflammation is unlikely as neuroinflammatory markers appear to remain ipsilateral in association with α-syn inclusion formation (Duffy et al., 2018b).

Importantly, ipsilateral-to-contralateral evolution of degeneration is not unique to the α-syn PFF model (Assous et al., 2014) and is observed if the duration of the experiment is long enough and the appropriate comparisons are made (e.g. use of control injected animals instead of the contralateral SNpc for quantitation). The α-syn PFF model serves to highlight this phenomenon by providing a stark contrast between nigral hemispheres in which only the ipsilateral SNpc accumulates α-syn.

Understanding the mechanism of contralateral degeneration in this model is important for two key reasons. First, effectively using the rat α-syn PFF model to vet neuroprotective strategies in future studies requires an understanding of whether or not nigrostriatal hemispheres

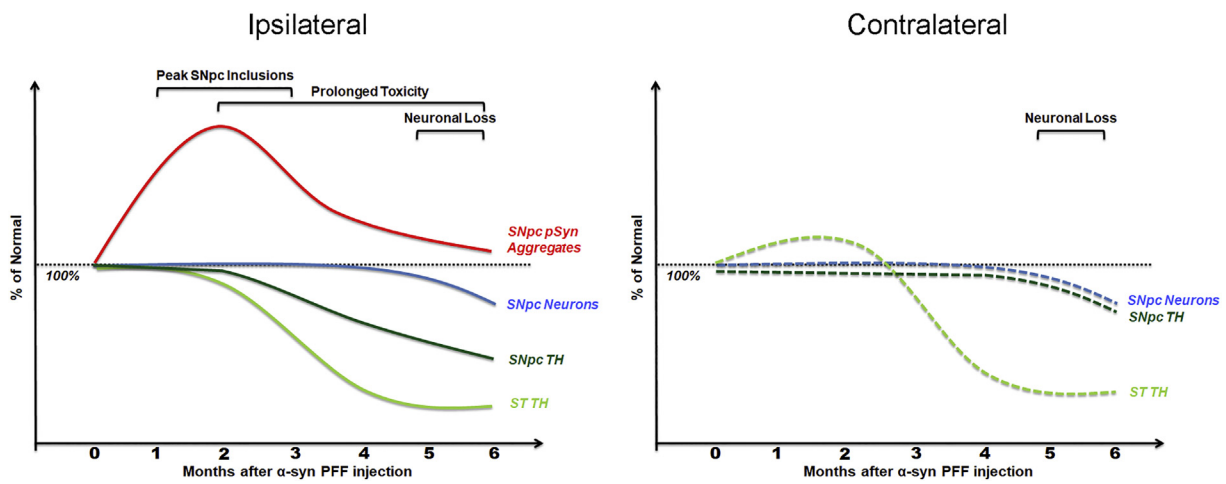

Fig. 10. Features of the PFF model. Graphic time course of phosphorylated alpha-synuclein (α-syn) at serine 129 (pSyn) containing neurons, tyrosine hydroxylase immunoreactive (THir) neurons in the substantia nigra pars compacta (SNpc), total neurons, and striatal TH. Ipsilateral (solid line) and contralateral (dashed line) are show for each.

degenerate via similar mechanisms. Second, the phenomenon of contralateral degeneration may represent a pathophysiological mechanism independent of the initiating insult, perhaps a pathophysiological mechanism that is common to multiple forms of sporadic PD. One possible factor driving this phenomenon is an intrahemispheric dopamine imbalance, but this hypothesis requires further investigation. At the time of PD diagnosis, patients present, almost without exception, with asymmetric nigrostriatal dysfunction which progresses over time to more severe symmetric nigrostriatal dysfunction (Marinus and van Hilten, 2015; Nandhagopal et al., 2009). It is possible that once a threshold of unilateral striatal dopamine depletion is reached, degeneration of the contralateral nigrostriatal circuitry is initiated. Indeed, previous studies have identified that the loss of dopamine can transform the basal ganglia into a destructive, excitotoxic network (Pedersen and Schmidt, 2000). Severe unilateral dopamine depletion results in bilateral increases in the firing rates of the subthalamic nucleus, pedunculopontine nucleus and SN pars reticulata (Breit et al., 2008). This increased firing rate may result in prolonged and enhanced glutamatergic input to contralateral SNpc neurons, resulting in excitotoxic cell death. Identification of the mechanism of contralateral nigral degeneration in the unilateral rat α-syn PFF model is the subject of ongoing study in our laboratory.

As motor deficits are a hallmark of PD, observing motor impairments would support the face validity of the PFF model of synucleinopathy. We observed modest motor deficits in the adjusting step task, an assessment of postural stability. Since postural instability is a core feature of PD, a measure of postural stability such as the adjusting step test could represent a suitable parallel for use in animal models. Importantly, the adjusting step task is not dependent upon asymmetry of degeneration which may explain why deficits were observed in the impacted forelimb corresponding to the more severely lesioned hemisphere. Indeed, we did not observe motor impairments in the majority of motor assessments we conducted. This is likely due to the fact that the magnitude of neurodegeneration is not sufficient to produce robust motor deficits, such as in overall mobility or individual fore or hindlimb step counts. The bilateral nature of the loss, can also be used to rationalize why tests designed to identify asymmetry caused by a unilateral lesion would not be effective, such as the cylinder task or previously used amphetamine-induced rotational asymmetry test that are commonly used in other asymmetric lesion models. It is likely that the degree of neurodegeneration needs to be increased in order to achieve motor impairments of adequate magnitude to be useful readouts in neuroprotective or dopamine replacement therapies. Ongoing studies are showing promise in this regard.

Rats injected bilaterally with α-syn PFFs also exhibited decreased stand and terminal dual stance times, as well as the increased average body speed and cadence compared to control rats. Collectively the direction of change in these metrics suggest that PFF-injected rats actually move faster. Other PD models, such as a rotenone-based rat model, display hyperactivity as well as motor impairment as assessed by rotarod and wire hang tests (Wrangel et al., 2015). Likewise, the MPTP neurotoxicant model, α-syn overexpression model, *LRRK2* (G2019S) and *SNCA* (A53T) genetic models show hyperactivity to some degree as a potential effect over time (Rousselet et al., 2003; Lam et al., 2011; Longo et al., 2014; Unger et al., 2006; Graham and Sidhu, 2010). PD is not simply just a motor disorder, though this is commonly the symptomatic features that are associated with the disease. Further assessment using cognitive and emotional reactivity tests are warranted, as these behavioral changes may be related to inclusions found in the cortex and or amygdala, rather than the nigrostriatal pathway.

In regards to the key features of PD, the present PFF model parameters result in robust α-syn pathology, neurodegeneration, and modest motor impairment. As a future direction, further optimization of the model is required to increase the number of inclusion containing neurons in order to augment nigral degeneration and produce robust motor behaviors. This may be achieved by increasing the portion of fibrils at the optimal length (~50 nm), further increasing the amount of PFFs injected, or adding additional injection site.

Currently, the PFF model provides a unique platform to study the progression of synucleinopathy. The PFF model has advantages and disadvantages when compared to other models (Volpicelli-Daley et al., 2016; Duffy et al., 2018a). As always, the selection of the model used should be appropriate to the questions the researcher is asking. The protracted timeframe leading to nigrostriatal degeneration and pathological features is consistent with idiopathic PD, with the exception of the atypical cytoplasmic pSyn in the striatum at later timepoints, and provides distinct windows of opportunity to test potential therapeutics (Fig. 10). For interventions aiming to focus on prevention of α-syn aggregation, the 0–2 month period of aggregate accumulation represents an appropriate time frame. If the goal of the intervention is to clear α-syn inclusions prior to degeneration, the endpoint focus should be at 2 months, when inclusion containing neurons are present at a high level. At the 3–4 month period, the TH phenotype is lost in the soma, but the neurons are still present, suggesting this is the latest critical timeframe to examine therapies that may provide neuroprotection from inclusion-associated degeneration. Changes in striatal TH, and the contralateral loss of nigral neurons also provide future targets to stem the progression of the synucleinopathy, Ultimately, knowledge of the

timing and magnitude of the pathophysiological events in the rat α-syn PFF model will provide critical guidance for appropriate use of this animal model platform to study synucleinopathy and potential disease-modifying therapies.

Supplementary data to this article can be found online at https://doi.org/10.1016/j.nbd.2019.104525.

Conflicts of interest

Authors have no conflicts of interest to disclose or competing interests in regards to data presented within this manuscript.

Summary statement

Simultaneous optimization of intrastriatal injection sites and quantity of alpha-synuclein preformed fibrils leads to marked increases in accumulation of phosphorylated alpha-synuclein inclusions, progressive nigrostriatal degeneration and motor deficits in rats.

Funding

This work was supported by The Michael J. Fox Foundation for Parkinson's Research, National Institute of Neurological Disorders and Stroke (NS099416) and the Weston Brain Institute.

References

Abdelmotilib, H., Maltbie, T., Delic, V., Liu, Z., Hu, X., Fraser, K.B., Moehle, M.S., Stoyka, L., Anabtawi, N., Krendelchtchikova, V., Volpicelli-Daley, L.A., West, A., 2017. Alpha-Synuclein fibril-induced inclusion spread in rats and mice correlates with dopaminergic Neurodegeneration. Neurobiol. Dis. 105, 84–98.

Assous, M., Had-Aissouni, L., Gubellini, P., Melon, C., Nafia, I., Salin, P., Kerkerian-Le-Goff, L., Kachidian, P., 2014. Progressive Parkinsonism by acute dysfunction of excitatory amino acid transporters in the rat substantia nigra. Neurobiol. Dis. 65, 69–81.

Blumenstock, S., Rodrigues, E.F., Peters, F., Blazquez-Llorca, L., Schmidt, F., Giese, A., Herms, J., 2017. Seeding and transgenic overexpression of alpha-synuclein triggers dendritic spine pathology in the neocortex. EMBO Mol. Med. 9 (5), 716–731.

Breit, S., Martin, A., Lessmann, L., Cerkez, D., Gasser, T., Schulz, J.B., 2008. Bilateral changes in neuronal activity of the basal ganglia in the unilateral 6-hydroxydopamine rat model. J. Neurosci. Res. 86, 1388–1396.

Chang, J.W., Wachtel, S.R., Young, D., Kang, U.J., 1999. Biochemical and anatomical characterization of forepaw adjusting steps in rat models of Parkinson's disease: studies on medial forebrain bundle and striatal lesions. Neuroscience 88, 617–628.

Dauer, W., Przedborski, S., 2003. Parkinson's disease: mechanisms and models. Neuron 39, 889–909.

Dijkstra, A.A., Ingrassia, A., de Menezes, R.X., van Kesteren, R.E., Rozemuller, A.J., Heutink, P., can de Berg, W.D., 2015. Evidence for immune response, axonal dysfunction and reduced endocytosis in the substantia Nigra in early stage Parkinson's disease. PLoS One 10 (6).

Dorsey, E.R., Constantinescu, R., Thompson, J.P., Biglan, K.M., Holloway, R.G., Kieburtz, K., Marshall, F.J., Ravina, B.M., Schifitto, G., Siderowf, A., Tanner, C.M., 2007. Projected number of people with Parkinson disease in the most populous nations, 2005 through 2030. Neurology 68, 384–386.

Duffy, M.F., Collier, T.J., Patterson, J.R., Kemp, C.J., Luke Fischer, D., Stoll, A.C., Sortwell, C.E., 2018a. Quality over quantity: advantages of using alpha-Synuclein preformed fibril triggered Synucleinopathy to model idiopathic Parkinson's disease. Front. Neurosci. 12, 621.

Duffy, M.F., Collier, T.J., Patterson, J.R., Kemp, C.J., Luk, K.C., Tansey, M.G., Paumier, K.L., Kanaan, N.M., Fischer, D.L., Polinski, N.K., Barth, O.L., Howe, J.W., Vaikath, N.N., Majbour, N.K., El-Agnaf, O.M.A., Sortwell, C.E., 2018b. Lewy body-like alpha-synuclein inclusions trigger reactive microgliosis prior to nigral degeneration. J. Neuroinflammation 15, 129.

Fahn, S., 2003. Description of Parkinson's disease as a clinical syndrome. Ann. N. Y. Acad. Sci. 991, 1–14.

Fleming, S.M., Salcedo, J., Fernagut, P.O., Rockenstein, E., Masliah, E., Levine, M.S., Chesselet, M.F., 2004. Early and progressive sensorimotor anomalies in mice over-expressing wild-type human alpha-synuclein. J. Neurosci. 24, 9434–9440.

Forno, L.S., DeLanney, L.E., Irwin, I., Langston, J.W., 1993. Similarities and differences between MPTP-induced parkinsonsim and Parkinson's disease. Neuropathologic considerations. Adv. Neurol. 60, 600–608.

Gombash, S.E., Manfredsson, F.P., Kemp, C.J., Kuhn, N.C., Fleming, S.M., Egan, A.E., Grant, L.M., Ciucci, M.R., MacKeigan, J.P., Sortwell, C.E., 2013. Morphological and behavioral impact of AAV2/5-mediated overexpression of human wildtype alpha-synuclein in the rat nigrostriatal system. PLoS One 8, e81426.

Gomez-Isla, T., Irizarry, M.C., Mariash, A., Cheung, B., Soto, O., Schrump, S., Sondel, J., Kotilinek, L., Day, J., Schwarzschild, M.A., Cha, J.H., Newell, K., Miller, D.W., Ueda, K., Young, A.B., Hyman, B.T., Ashe, K.H., 2003. Motor dysfunction and gliosis with preserved dopaminergic markers in human alpha-synuclein A30P transgenic mice. Neurobiol. Aging 24, 245–258.

Graham, D.R., Sidhu, A., 2010. Mice expressing the A53T mutant form of human alpha-synuclein exhibit hyperactivity and reduced anxiety-like behavior. J. Neurosci. Res. 88, 1777–1783.

Grassi, D., Howard, S., Zhou, M., Diaz-Perez, N., Urban, N.T., Guerrero-Given, D., Kamasawa, N., Volpicelli-Daley, L.A., Lograsso, P., Lasmezas, C.I., 2018. Identification of a highly neurotoxic α-synuclein species inducing mitochondrial damage and mithophagy in Parkinson's disease. Proc Natl Acad Sci USA 13 115 (11), E2634–E2643.

Grassi, D., Diaz-Perez, N., Volpicelli-Daley, L.A., Lasmezas, C.I., 2019. Pα-syn* mitotoxicity is lined to MAPK activation and involves tau phosphorylation and aggregation at the mitochondria. Neurobiol. Dis. 124, 248–262.

Graybiel, A.M., Hirsch, E.C., Agid, Y., 1990. The nigrostriatal system in Parkinson's disease. Adv. Neurol. 53, 17–29.

Grundemann, J., Schlaudraff, F., Haeckel, O., Liss, B., 2008. Elevated alpha-synuclein mRNA levels in individual UV-laser-microdissected dopaminergic substantia nigra neurons in idiopathic Parkinson's disease. Nucleic Acids Res. 36, e38.

Ip, C.W., Klaus, L.C., Karikari, A.A., Visanji, N.P., Brotchie, J.M., Lang, A.E., Volkmann, J., Koprich, J.B., 2017. AAV1/2-induced overexpression of A53T-alpha-synuclein in the substantia nigra results in degeneration of the nigrostriatal system with Lewy-like pathology and motor impairment: a new mouse model for Parkinson's disease. Acta neuropathologica communications 5, 11.

Jankovic, J., 2008. Parkinson's disease: clinical features and diagnosis. J. Neurol. Neurosurg. Psychiatry 79, 368–376.

Kingsbury, A.E., Daniel, S.E., Sangha, H., Eisen, S., Lees, A.J., Foster, O.J., 2004. Alteration in alpha-synuclein mRNA expression in Parkinson's disease. Mov. Disord. 19, 162–170.

Kirik, D., Rosenblad, C., Burger, C., Lundberg, C., Johansen, T.E., Muzyczka, N., Mandel, R.J., Bjorklund, A., 2002. Parkinson-like neurodegeneration induced by targeted overexpression of alpha-synuclein in the nigrostriatal system. J. Neurosci. 22, 2780–2791.

Klein, R.L., King, M.A., Hamby, M.E., Meyer, E.M., 2002. Dopaminergic cell loss induced by human A30P alpha-synuclein gene transfer to the rat substantia nigra. Hum. Gene Ther. 13, 605–612.

Kordower, J.H., Olanow, C.W., Dodiya, H.B., Chu, Y., Beach, T.G., Adler, C.H., Halliday, G.M., Bartus, R.T., 2013. Disease duration and the integrity of the nigrostriatal system in Parkinson's disease. Brain J. Neurol. 136, 2419–2431.

Lam, H.A., Wu, N., Cely, I., Kelly, R.L., Hean, S., Richter, F., Magen, I., Cepeda, C., Ackerson, L.C., Walwyn, W., Masliah, E., Chesselet, M.F., Levine, M.S., Maidment, N.T., 2011. Elevated tonic extracellular dopamine concentration and altered dopamine modulation of synaptic activity precede dopamine loss in the striatum of mice overexpressing human alpha-synuclein. J. Neurosci. Res. 89, 1091–1102.

Lerner, T.N., Shilyansky, C., Davidson, T.J., Evans, K.E., Beier, K.T., Zalocusky, K.A., Crow, A.K., Malenka, R.C., Luo, L., Tomer, R., Deisseroth, K., 2015. Intact-brain analyses reveal distinct information carried by SNc dopamine subcircuits. Cell 162, 635–647.

Leys, C., Ley, C., Klein, O., Bernard, P., Licata, L., 2013. Detecting outliers: do not use standard deviation around the mean, use absolute deviation around the median. J. Exp. Soc. Psychol. 49 (4), 764–766.

Lo Bianco, C., Ridet, J.L., Schneider, B.L., Deglon, N., Aebischer, P., 2002. Alpha -Synucleinopathy and selective dopaminergic neuron loss in a rat lentiviral-based model of Parkinson's disease. Proc. Natl. Acad. Sci. U. S. A. 99, 10813–10818.

Longo, F., Russo, I., Shimshek, D.R., Greggio, E., Morari, M., 2014. Genetic and pharmacological evidence that G2019S LRRK2 confers a hyperkinetic phenotype, resistant to motor decline associated with aging. Neurobiol. Dis. 71, 62–73.

Luk, K.C., Kehm, V., Carroll, J., Zhang, B., O'Brien, P., Trojanowski, J.Q., Lee, V.M., 2012. Pathological alpha-synuclein transmission initiates Parkinson-like neurodegeneration in nontransgenic mice. Science 338, 949–953.

Luk, K.C., Covell, D.J., Kehm, V.M., Zhang, B., Song, I.Y., Byrne, M.D., Pitkin, R.M., Decker, S.C., Trojanowski, J.Q., Lee, V.M., 2016. Molecular and biological compatibility with host alpha-Synuclein influences fibril pathogenicity. Cell Rep. 16, 3373–3387.

Lundblad, M., Decressac, M., Mattsson, B., Bjorklund, A., 2012. Impaired neurotransmission caused by overexpression of alpha-synuclein in nigral dopamine neurons. Proc. Natl. Acad. Sci. U. S. A. 109, 3213–3219.

Marinus, J., van Hilten, J.J., 2015. The significance of motor (a)symmetry in Parkinson's disease. Mov. Disord. 30, 379–385.

Marras, C., Beck, J.C., Bower, J.H., Roberts, E., Ritz, B., Ross, G.W., Abbott, R.D., Savica, R., Van Den Eeden, S.K., Willis, A.W., Tanner, C.M., Parkinson's Foundation PG, 2018. Prevalence of Parkinson's disease across North America. NPJ Parkinson's Dis. 4, 21.

Matsuoka, Y., Vila, M., Lincoln, S., McCormack, A., Picciano, M., LaFrancois, J., Yu, X., Dickson, D., Langston, W.J., McGowan, E., Farrer, M., Hardy, J., Duff, K., Przedborski, S., Di Monte, D.A., 2001. Lack of nigral pathology in transgenic mice expressing human alpha-synuclein driven by the tyrosine hydroxylase promoter. Neurobiol. Dis. 8, 535–539.

Mulcahy, P., O'Doherty, A., Paucard, A., O'Brien, T., Kirik, D., Dowd, E., 2012. Development and characterisation of a novel rat model of Parkinson's disease induced by sequential intranigral administration of AAV-alpha-synuclein and the pesticide, rotenone. Neuroscience 203, 170–179.

Munoz, P., Paris, I., Segura-Aguilar, J., 2016. Corrigendum: commentary: evaluation of models of Parkinson's disease. Front. Neurosci. 10, 320.

Nandhagopal, R., Kuramoto, L., Schulzer, M., Mak, E., Cragg, J., Lee, C.S., McKenzie, J., McCormick, S., Samii, A., Troiano, A., Ruth, T.J., Sossi, V., de la Fuente-Fernandez,

R., Calne, D.B., Stoessl, A.J., 2009. Longitudinal progression of sporadic Parkinson's disease: a multi-tracer positron emission tomography study. Brain 132, 2970–2979.
Neystat, M., Lynch, T., Przedborski, S., Kholodilov, N., Rzhetskaya, M., Burke, R.E., 1999. Alpha-synuclein expression in substantia nigra and cortex in Parkinson's disease. Mov. Disord. 14, 417–422.
Nuber, S., Harmuth, F., Kohl, Z., Adame, A., Trejo, M., Schonig, K., Zimmermann, F., Bauer, C., Casadei, N., Giel, C., Calaminus, C., Pichler, B.J., Jensen, P.H., Muller, C.P., Amato, D., Kornhuber, J., Teismann, P., Yamakado, H., Takahashi, R., Winkler, J., Masliah, E., Riess, O., 2013. A progressive dopaminergic phenotype associated with neurotoxic conversion of alpha-synuclein in BAC-transgenic rats. Brain 136, 412–432.
Oliveras-Salva, M., Van der Perren, A., Casadei, N., Stroobants, S., Nuber, S., D'Hooge, R., Van den Haute, C., Baekelandt, V., 2013. rAAV2/7 vector-mediated overexpression of alpha-synuclein in mouse substantia nigra induces protein aggregation and progressive dose-dependent neurodegeneration. Mol. Neurodegener. 8, 44.
Olsson, M., Nikkhah, G., Bentlage, C., Bjorklund, A., 1995. Forelimb akinesia in the rat Parkinson model: differential effects of dopamine agonists and nigral transplants as assessed by a new stepping test. J. Neurosci. 15, 3863–3875.
Osterberg, V.R., Spinelli, K.J., Weston, L.J., Luk, K.C., Woltjer, R.L., Unni, V.K., 2015. Progressive aggregation of alpha-synuclein and selective degeneration of lewy inclusion-bearing neurons in a mouse model of parkinsonism. Cell Rep. 10, 1252–1260.
Paumier, K.L., Luk, K.C., Manfredsson, F.P., Kanaan, N.M., Lipton, J.W., Collier, T.J., Steece-Collier, K., Kemp, C.J., Celano, S., Schulz, E., Sandoval, I.M., Fleming, S., Dirr, E., Polinski, N.K., Trojanowski, J.Q., Lee, V.M., Sortwell, C.E., 2015. Intrastriatal injection of pre-formed mouse alpha-synuclein fibrils into rats triggers alpha-synuclein pathology and bilateral nigrostriatal degeneration. Neurobiol. Dis. 82, 185–199.
Pedersen, V., Schmidt, W.J., 2000. The neuroprotectant properties of glutamate antagonists and antiglutamatergic drugs. Neurotox. Res. 2, 179–204.
Polinski, N.K., Volpicelli-Daley, L.A., Sortwell, C.E., Luk, K.C., Cremades, N., Gottler, L.M., Froula, J., Duffy, M.F., Lee, V.M.Y., Martinez, T.N., Dave, K.D., 2018. Best practices for generating and using alpha-Synuclein pre-formed fibrils to model Parkinson's disease in rodents. J. Park. Dis. 8, 303–322.
Pollanen, M.S., Dickson, D.W., Bergeron, C., 1993. Pathology and biology of the Lewy body. J. Neuropathol. Exp. Neurol. 52, 183–191.
Potashkin, J.A., Blume, S.R., Runkle, N.K., 2010. Limitations of animal models of Parkinson's disease. Parkinson's disease 2011, 658083.
Rousselet, E., Joubert, C., Callebert, J., Parain, K., Tremblay, L., Orieux, G., Launay, J.M., Cohen-Salmon, C., Hirsch, E.C., 2003. Behavioral changes are not directly related to striatal monoamine levels, number of nigral neurons, or dose of parkinsonian toxin MPTP in mice. Neurobiol. Dis. 14, 218–228.
Schallert, T., 2006. Behavioral tests for preclinical intervention assessment. NeuroRx 3, 497–504.
Schallert, T., Fleming, S.M., Leasure, J.L., Tillerson, J.L., Bland, S.T., 2000. CNS plasticity and assessment of forelimb sensorimotor outcome in unilateral rat models of stroke, cortical ablation, parkinsonism and spinal cord injury. Neuropharmacology 39, 777–787.
Spillantini, M.G., Schmidt, M.L., Lee, V.M., Trojanowski, J.Q., Jakes, R., Goedert, M., 1997. Alpha-synuclein in Lewy bodies. Nature 388, 839–840.
Su, X., Fischer, D.L., Li, X., Bankiewicz, K., Sortwell, C.E., Federoff, H.J., 2017. Alpha-Synuclein mRNA is not increased in sporadic PD and alpha-Synuclein accumulation does not block GDNF signaling in Parkinson's disease and disease models. Mol. Ther. 25, 2231–2235.
Tan, E.K., Chandran, V.R., Fook-Chong, S., Shen, H., Yew, K., Teoh, M.L., Yuen, Y., Zhao, Y., 2005. Alpha-synuclein mRNA expression in sporadic Parkinson's disease. Mov. Disord. 20, 620–623.
Tarutani, A., Suzuki, G., Shimozawa, A., Nonaka, T., Akiyama, H., Hisanaga, S., Hasegawa, M., 2016. The effect of fragmented pathogenic alpha-Synuclein seeds on prion-like propagation. J. Biol. Chem. 291, 18675–18688.
Ulusoy, A., Decressac, M., Kirik, D., Bjorklund, A., 2010. Viral vector-mediated overexpression of alpha-synuclein as a progressive model of Parkinson's disease. Prog. Brain Res. 184, 89–111.
Unger, E.L., Eve, D.J., Perez, X.A., Reichenbach, D.K., Xu, Y., Lee, M.K., Andrews, A.M., 2006. Locomotor hyperactivity and alterations in dopamine neurotransmission are associated with overexpression of A53T mutant human alpha-synuclein in mice. Neurobiol. Dis. 21, 431–443.
Vaikath, N.N., Majbour, N.K., Paleologou, K.E., Ardah, M.T., van Dam, E., van de Berg, W.D., Forrest, S.L., Parkkinen, L., Gai, W.P., Hattori, N., Takanashi, M., Lee, S.J., Mann, D.M., Imai, Y., Halliday, G.M., Li, J.Y., El-Agnaf, O.M., 2015. Generation and characterization of novel conformation-specific monoclonal antibodies for alpha-synuclein pathology. Neurobiol. Dis. 79, 81–99.
Van der Perren, A., Van den Haute, C., Baekelandt, V., 2015. Viral vector-based models of Parkinson's disease. Curr. Top. Behav. Neurosci. 22, 271–301.
Volpicelli-Daley, L.A., Luk, K.C., Patel, T.P., Tanik, S.A., Riddle, D.M., Stieber, A., Meaney, D.F., Trojanowski, J.Q., Lee, V.M., 2011. Exogenous alpha-synuclein fibrils induce Lewy body pathology leading to synaptic dysfunction and neuron death. Neuron 72, 57–71.
Volpicelli-Daley, L.A., Luk, K.C., Lee, V.M., 2014. Addition of exogenous alpha-synuclein preformed fibrils to primary neuronal cultures to seed recruitment of endogenous alpha-synuclein to Lewy body and Lewy neurite-like aggregates. Nat. Protoc. 9, 2135–2146.
Volpicelli-Daley, L.A., Kirik, D., Stoyka, L.E., Standaert, D.G., Harms, A.S., 2016. How can rAAV-alpha-synuclein and the fibril alpha-synuclein models advance our understanding of Parkinson's disease? J. Neurochem. 139 (Suppl. 1), 131–155.
Wall, N.R., De La Parra, M., Callaway, E.M., Kreitzer, A.C., 2013. Differential innervation of direct- and indirect-pathway striatal projection neurons. Neuron 79, 347–360.
von Wrangel, C., Schwabe, K., John, N., Krauss, J.K., Alam, M., 2015. The rotenone-induced rat model of Parkinson's disease: behavioral and electrophysiological findings. Behav. Brain Res. 279, 52–61.
Yamada, M., Iwatsubo, T., Mizuno, Y., Mochizuki, H., 2004. Overexpression of alpha-synuclein in rat substantia nigra results in loss of dopaminergic neurons, phosphorylation of alpha-synuclein and activation of caspase-9: resemblance to pathogenetic changes in Parkinson's disease. J. Neurochem. 91, 451–461.
Zeiss, C.J., Allore, H.G., Beck, A.P., 2017. Established patterns of animal study design undermine translation of disease-modifying therapies for Parkinson's disease. PLoS One 12, e0171790.
Zhou, J., Broe, M., Huang, Y., Anderson, J.P., Gai, W.P., Milward, E.A., Porritt, M., Howells, D., Hughes, A.J., Wang, X., Halliday, G.M., 2011. Changes in the solubility and phosphorylation of alpha-synuclein over the course of Parkinson's disease. Acta Neuropathol. 121, 695–704.